ANALYSIS OF EMULSION RUN0 DATA OF THE SND@LHC EXPERIMENT AT THE CERN-LHC

A THESIS SUBMITTED TO
THE GRADUATE SCHOOL OF NATURAL AND APPLIED SCIENCES
OF
MIDDLE EAST TECHNICAL UNIVERSITY

BY

EDA YAMAN

IN PARTIAL FULFILLMENT OF THE REQUIREMENTS
FOR
THE DEGREE OF MASTER OF SCIENCE
IN
PHYSICS

SEPTEMBER 2023

Approval of the thesis:

ANALYSIS OF EMULSION RUN0 DATA OF THE SND@LHC EXPERIMENT AT THE CERN-LHC

submitted by **EDA YAMAN** in partial fulfillment of the requirements for the degree of **Master of Science in Physics Department, Middle East Technical University** by,

Prof. Dr. Halil Kalıpçılar
Dean, Graduate School of **Natural and Applied Sciences** _____

Prof. Dr. Seçkin Kürkçüoğlu
Head of Department, **Physics** _____

Prof. Dr. Ali Murat Güler
Supervisor, **Physics, METU** _____

Examining Committee Members:

Prof. Dr. İsmail Turan
Physics, METU _____

Prof. Dr. Ali Murat Güler
Physics, METU _____

Prof. Dr. Antonia Di Crescenzo
Physics, University of Naples Federico II _____

Date:11.09.2023

I hereby declare that all information in this document has been obtained and presented in accordance with academic rules and ethical conduct. I also declare that, as required by these rules and conduct, I have fully cited and referenced all material and results that are not original to this work.

Name, Surname: EDA YAMAN

Signature :

ABSTRACT

ANALYSIS OF EMULSION RUN0 DATA OF THE SND@LHC EXPERIMENT AT THE CERN-LHC

YAMAN, EDA
M.S., Department of Physics
Supervisor: Prof. Dr. Ali Murat Güler

SEPTEMBER 2023, 67 pages

SND@LHC is a compact and stand-alone experiment that covers the pseudo-rapidity region of $7.2 < \eta < 8.4$, inaccessible to the other experiments at the Large Hadron Collider (LHC). It has the potential to make significant contributions to neutrino physics in a previously unexplored high-energy region between 350 GeV and 10 TeV and the physics beyond the Standard Model. The SND@LHC "Emulsion RUN0" setup was designed to test data reconstruction processes' performance, including emulsion scanning and subsequent reconstruction steps. Through the use of this test setup, the experiment can determine the efficiency and precision of linking, alignment, tracking, and vertexing algorithms. In this thesis work, the Emulsion RUN0 Data is analyzed, and new selection criteria on the track and vertex reconstruction are applied to improve the tracking and vertexing. A significant reduction in the number of false tracks and vertices was obtained while improving the vertex quality in terms of impact parameter and multiplicity distributions.

Keywords: SND@LHC Experiment, Emulsion, Neutrino interactions

ÖZ

CERN-LHC'DEKİ SND@LHC DENEYİNİN EMÜLSİYON RUN0 VERİ ANALİZİ

YAMAN, EDA
Yüksek Lisans, Fizik Bölümü
Tez Yöneticisi: Prof. Dr. Ali Murat Güler

Eylül 2023 , 67 sayfa

SND@LHC, Büyük Hadron Çarpıştırıcısı'ndaki (BHÇ) diğer deneylerin ulaşamadığı $7.2 < \eta < 8.4$ sözde hızlılık aralığında ölçümler yapabilen kompakt bir deneydir. Daha önce keşfedilmemiş yüksek enerji bölgesinde, 350 GeV ile 10 TeV, nötrino fiziği araştırmaları ve Standart Model ötesi fizik çalışmaları yapma potansiyeline sahiptir. SND@LHC "Emülsiyon RUN0" düzeneği, emülsiyon tarama ve sonrasındaki veri yapılandırma adımlarının verimliliğini test etmek için tasarlanmıştır. Bu test düzeneğinin kullanılmasıyla deney, hizalama, iz yapılandırma ve etkileşim noktası belirleme algoritmalarının verimliliğini ve doğruluğunu belirleyebilir. Bu tez çalışmasında, Emülsiyon RUN0 verisi analiz edilmiş ve iz ve vörteks yapılandırma performasının iyileştirilmesi için yeni seçim kriterleri geliştirilmiştir. Vörteks kalitesi etki parametresi ve çokluk dağılımları açısından iyileştirilmiş ve sahte iz ve vörteks sayısında önemli bir azalma elde edilmiştir.

Anahtar Kelimeler: SND@LHC Deneyi, Emülsiyon, Nötrino etkileşimleri

To my family and Başak Yaren Fidan.

ACKNOWLEDGMENTS

I would like to thank TENMAK and CERN for supporting our project (Grant No. 2022TENMAK(CERN)A5.H3.F2-1). I would also like to express my deep gratitude to all collaboration members of the SND@LHC project, especially Antonia Di Crescenzo, Antonio Iuliano, and Fabio Alicante, who stood out with their helpful attitudes and provided support with their expertise and knowledge. Furthermore, I would like to sincerely thank my friends, Onur Durhan and Cemal Dinç, members of the METU SND@LHC team, for their invaluable support. Also, I would like to express my gratitude to my close friend Ceren Yazıcı and her family, who have been with me during every challenging moment and generously provided their support. I would like to convey my heartfelt thanks to my dear mother and father, Dilek and Hasan, and my lovely brother Alperen, who have guided and supported me at every step of my life, particularly during this study. I would like to dedicate this study of mine to the memory of my cousin Başak Yaren Fidan, who tragically lost her life in the February 6, 2023 earthquake while she was a physics student at Istanbul University, carrying the aspiration of becoming a successful physicist. And especially, I would like to offer my special thanks to Prof. Dr. Ali Murat Güler, who illuminated my path with his profound experience and wisdom at every stage of the work, guiding me and providing support during my study.

TABLE OF CONTENTS

LIST OF TABLES

TABLES

LIST OF FIGURES

FIGURES

LIST OF ABBREVIATIONS

SND@LHC	The Scattering and Neutrino Detector at the LHC
LHC	The Large Hadron Collider
CERN	The European Organization for Nuclear Research
SM	Standard Model
ATLAS	A Toroidal LHC ApparatuS
IP1	Interaction Point 1
METU	Middle East Technical University
DIS	Deep Inelastic Scattering
pp	proton-proton
LHCb	The Large Hadron Collider beauty
PDF	Parton Distribution Function
LFU	Lepton Flavour Universality
CC	Charged Current
NC	Neutral Current
NuTeV	Neutrinos at the Tevatron
CHORUS	CERN Hybrid Oscillation Research apparatus
OPERA	The Oscillation Project with Emulsion-tRacking Apparatus
SiPM	Silicon Photomultiplier
ECC	Emulsion Cloud Chamber
FIP	Feebly Interacting Particles
MIP	Minimum Ionizing Particles
ESS	The European Scanning System
LASSO	Large Angle Scanning System for OPERA
FEDRA	Framework for Emulsion Data Reconstruction and Analysis

3D	Three-Dimensional
MC	Monte Carlo

CHAPTER 1

INTRODUCTION

Neutrinos, known for their feeble interactions, have been a subject of significant scientific interest due to their potential to probe the fundamental principles of particle physics. Neutrino interactions have mainly been measured for neutrino oscillation research in the energy range below 350 GeV over the last few decades. However, the IceCube (The IceCube Neutrino Observatory) collaboration has reported detecting a few tens of events in the 10 TeV to 1 PeV energy range [2]. Nonetheless, the range between 350 GeV and 10 TeV remained uncharted [7].

Observing neutrino interactions in the previously uncharted energy range of a few hundred GeV to a few TeV in a laboratory is made possible by LHC neutrinos. The LHC neutrino flux also receives a remarkable contribution from the τ flavour. Approximately thirty years ago, it was first proposed to use the LHC as a neutrino factory, also for the undiscovered tau neutrino [8][13]. At the LHC, the high intensity of proton-proton collisions produces a significant forward neutrino flux, and the high neutrino energies yield comparatively large neutrino cross-sections.

The SND@LHC experiment fills this crucial information gap by stepping into the undiscovered region of high-energy neutrinos, offering an exceptional opportunity for precise SM testing and research of new physics. SND@LHC is a compact, standalone neutrino detector that is placed 480 meters distant from the ATLAS interaction point downstream of Interaction Point 1 (IP1) in the unused TI18 tunnel [2].

In order to increase the neutrino flux from decays of charmed particles, which is essential for measuring charm production using electron neutrino events, SND@LHC uses an off-axis setup. The off-axis positioning also enables the search for Lepton

Flavour Universality violation by allowing for the partial cancellation of production uncertainties when measuring ratios of different flavour neutrino cross-sections. This off-axis position in the pseudo-rapidity range of $7.2 < \eta < 8.4$ complements current LHC experiments by revealing important details about neutrino features and interactions in an unexplored kinematic region. With an energy range of 100 GeV to a few TeV, SND@LHC is designed to measure high-energy neutrinos and has the ability to efficiently identify the three neutrino flavours (electron neutrino, muon neutrino, and tau neutrino) [2].

During the Long Shutdown 2 of LHC, the SND@LHC detector was installed in TI18, and it received its first data in July 2022 [3]. The experiment's first phase involves running the detector continuously throughout LHC Run 3 to obtain a total integrated luminosity of around 250 fb^{-1} in 2022–2025. The experiment has been collecting data successfully throughout the proton physics run of 2022. The METU SND@LHC team is a part of the SND@LHC Collaboration and contributes to the experiment in various respects.

The data reconstruction quality is critical to the success of the SND@LHC investigation; thus, it is essential to carefully test the data reconstruction algorithms to achieve this. The experiment encountered difficulties during the initial months after the detector was installed because of the low integrated luminosity caused by the commissioning and scrubbing of the beam. As a result, just one detector brick out of twenty had 57 emulsion films installed between April 7 and July 26, 2022. In order to optimize the use of emulsion films, the other bricks were filled only with tungsten plates. This setup is called the "Emulsion RUN0" setup. In this thesis work, the performance of data reconstruction procedures, including emulsion scanning and subsequent reconstruction phases, was studied using the data acquired with the SND@LHC "Emulsion RUN0" setup at the LHC Run3. Using this test setup, the efficiency and accuracy of linking, alignment, tracking, and vertexing algorithms were tested. These procedures are essential for reconstructing particle tracks and finding their interaction points. For these reasons, the Emulsion RUN0 data was analyzed in this thesis work, which will be discussed in Chapter 4.

The general concepts of the following chapters can be summarized as follows;

- In Chapter 2, the main physics motivation of the SND@LHC will be discussed.
- In Chapter 3, the SND@LHC detector layout will be introduced.
- In Chapter 4, the Emulsion RUN0 setup, the emulsion data reconstruction, and the analysis of Emulsion RUN0 data will be introduced in detail.
- In Chapter 5, the results of the analysis will be discussed.

CHAPTER 2

PHYSICS MOTIVATION

The SND@LHC experiment is inspired by two main aspects that make it both practical and exciting to build a compact neutrino detector at the Large Hadron Collider (LHC) [2]. The LHC's high luminosity from proton-proton collisions produces a significant neutrino flux in the forward direction, and these neutrinos have relatively large neutrino cross-sections due to their high energy. These two factors and the detector's very small size have a significant physics potential.

SND@LHC also provides a direct search for Feebly Interacting Particles (FIP), which is a developing field of study. These particles interact with matter extremely rarely, through weak or gravitational interactions, because they are either incredibly light or have exceedingly long lifetimes. Investigating FIPs is particularly fascinating since it may reveal the origins of cosmic inflation, matter anti-matter asymmetry, and dark matter, among other cosmological puzzles. When particles scatter at the LHC interaction point, they may produce FIPs, which might pass through the SND@LHC detector and scatter within. Because of its unique design, the SND@LHC detector can distinguish between interactions involving FIPs and those involving neutrinos.

The experiment takes advantage of the unique properties of high-energy neutrinos produced by the LHC. The detection of electron neutrinos and anti-neutrinos is mostly due to charmed-hadron decays in the pseudo-rapidity range, which will be investigated by SND@LHC. The observation of electron neutrinos and anti-neutrinos provides indirect measurements of charmed-hadron production. SND@LHC aims to determine charmed-hadron production cross-section with an accuracy of approximately 35% [2]. The results obtained will be useful in the constraint of the gluon parton density function in a region of very small x, which is important for experiments at future

accelerators.

As a bridge between accelerator and astroparticle physics, the results of SND@LHC are also important for predicting high-energy neutrinos generated in cosmic-ray interactions. It is possible to probe several Standard Model (SM) features and investigate new physics beyond its predictions due to having the ability to measure neutrino scattering and interactions. Moreover, astrophysical neutrinos provide significant information regarding non-thermal sources in the Universe.

Most neutrino interactions have been observed at energies below 350 GeV in recent decades, with IceCube observations extending to energies ranging from 10 TeV to 1 PeV [2]. However, the energy range between 350 GeV and 10 TeV is mostly unexplored, as shown in Figure 2.1. The aim of SND@LHC is to close this knowledge gap by detecting and researching neutrino interactions in this unexplored energy range in a laboratory environment.

In proton-proton interactions at the LHC, neutrinos are produced through prompt leptonic W and Z decays, b and c decays, and following decays of pions (π) and kaons (K) [4]. ν_es and $\bar{\nu_e}$s are mainly produced in charmed hadron decays, with small contamination from kaons at low energies where the interaction cross-section with the detector is lower. ν_τs and $\bar{\nu_\tau}$s are formed exclusively by heavy-hadron decays. Pion and kaon decays contribute significantly to muon (anti) neutrinos.

Having a softer energy spectrum in the studied pseudo-rapidity region, muon neutrinos from charm and pion or kaon decays can be distinguished by neutrino energy measurements. The flux of different neutrino and anti-neutrino flavours in the (η, E_ν) plane is shown in Figure 2.2.

The neutrino yield of the experiment depends on the flux and cross-section of neutrino interactions. The main uncertainty in the flux of neutrinos coming from heavy quarks lies in the production. Therefore, analyzing the high-energy neutrinos offers a clear understanding of heavy-flavour production.

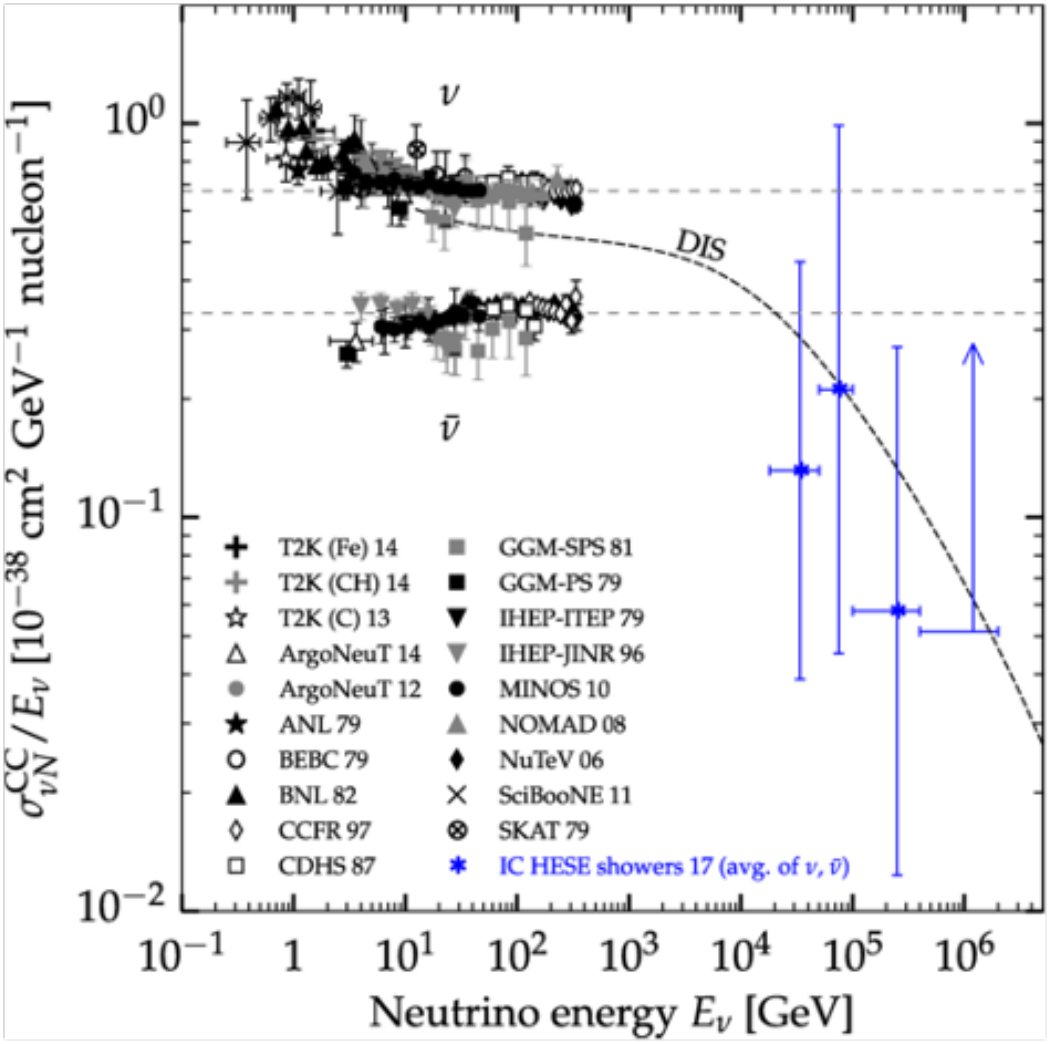

Figure 2.1: Available neutrino cross-section measurements. The predicted rate of DIS interaction is represented by the dashed curve [2].

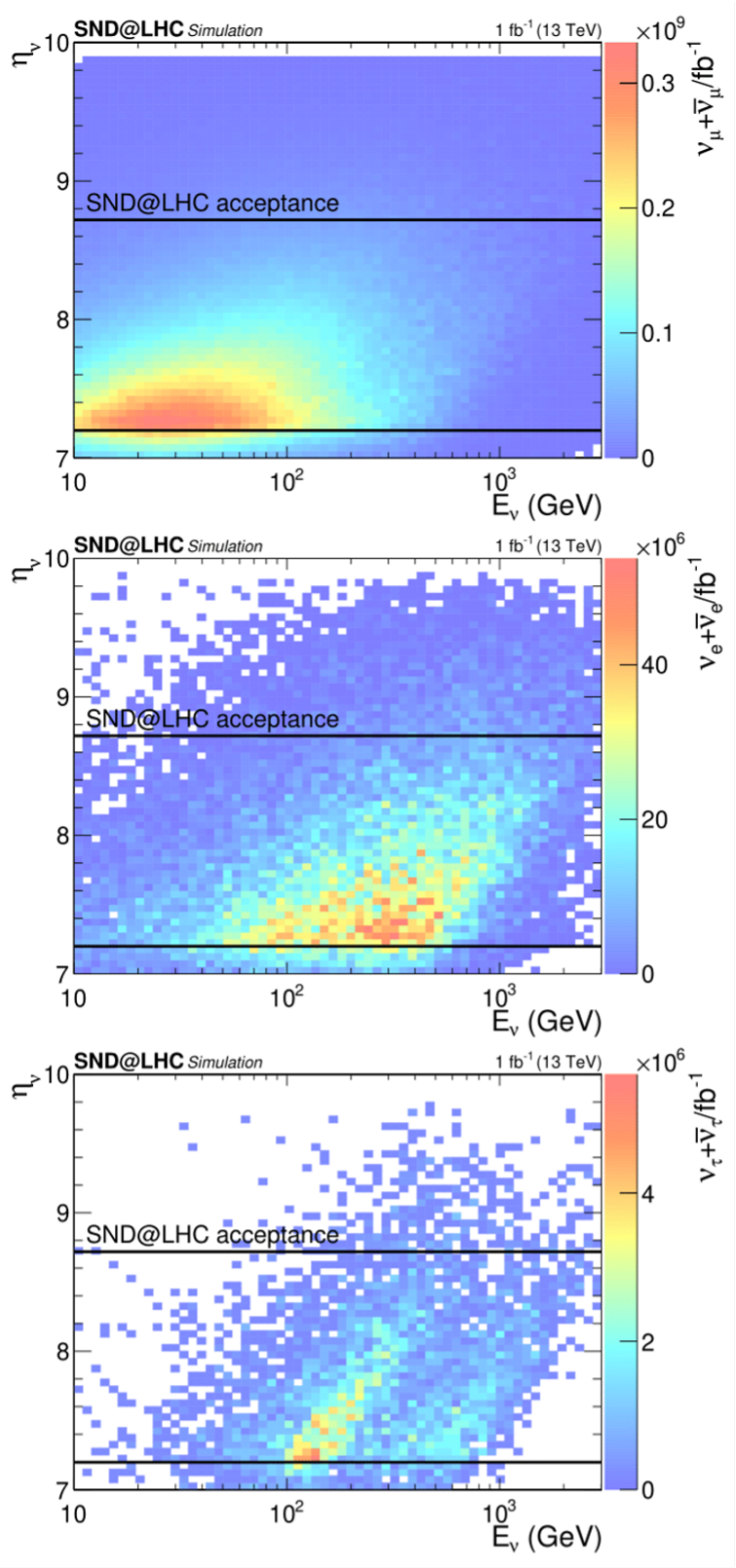

Figure 2.2: ν and $\bar{\nu}$ flux as a function of ν energy E_ν and pseudo-rapidity η_ν for ν_μ (top), ν_e (middle) and ν_τ (bottom) [2].

2.1 Charmed-hadron production in pp collisions

Hadrons are composite particles composed of quarks, the fundamental particles which constitute matter. There are six flavours of quarks: up, down, charm, strange, top, and bottom. One of the heavier quarks is the charm quark, and hadrons that contain the charm quark are known as "charmed hadrons." Charmed hadrons are divided into two main groups: charmed mesons and charmed baryons. Mesons are hadrons consisting of a quark and an antiquark. Charmed mesons are composed of a charm quark and a lighter antiquark, usually an up or a down antiquark. The D mesons, such as the D^0 $(c\bar{u})$ meson and the D^+ $(c\bar{d})$ meson, are the most well-known charmed mesons. Baryons are hadrons consisting of three quarks. Charmed baryons are composed of a charm quark and two lighter quarks. The Λ_c^+ (udc) baryon is an example of a charmed baryon.

Charmed hadrons are typically produced in collisions between high-energy particles, such as those in particle accelerators like the LHC. The decay of charmed hadrons originating in the LHC pp collisions is the primary source of the electron neutrinos and anti-neutrinos interacting in SND@LHC [2]. Therefore, measuring electron flux on experiment acceptance can illuminate the heavy-quark production in an uncharted region.

The production of charmed hadrons in pp collisions has been studied at LHC at lower pseudo-rapidity. The LHCb has measured charm and beauty production in the pseudo-rapidity region $\eta < 4.5$, which is the closest range to the SND@LHC [2]. The energy spectrum of incoming neutrinos and anti-neutrinos in the SND@LHC detector's pseudo-rapidity range, 7.2 to 8.4, normalized to 250 fb^{-1}, is shown in Figure 2.3. Charmed-hadron decays are the main source of electron neutrinos and anti-neutrinos in this energy range. As a consequence, by observing electron neutrinos and anti-neutrinos, SND@LHC may indirectly measure the production of charmed hadrons.

The FLUKA simulation predicts that 10% of the ν_es and $\bar{\nu_e}$s interacting in the detector come from kaon decays, especially from K^0s, and have energy below 200 GeV [2]. The Pythia8 event generator has been used to estimate the beauty-hadron de-

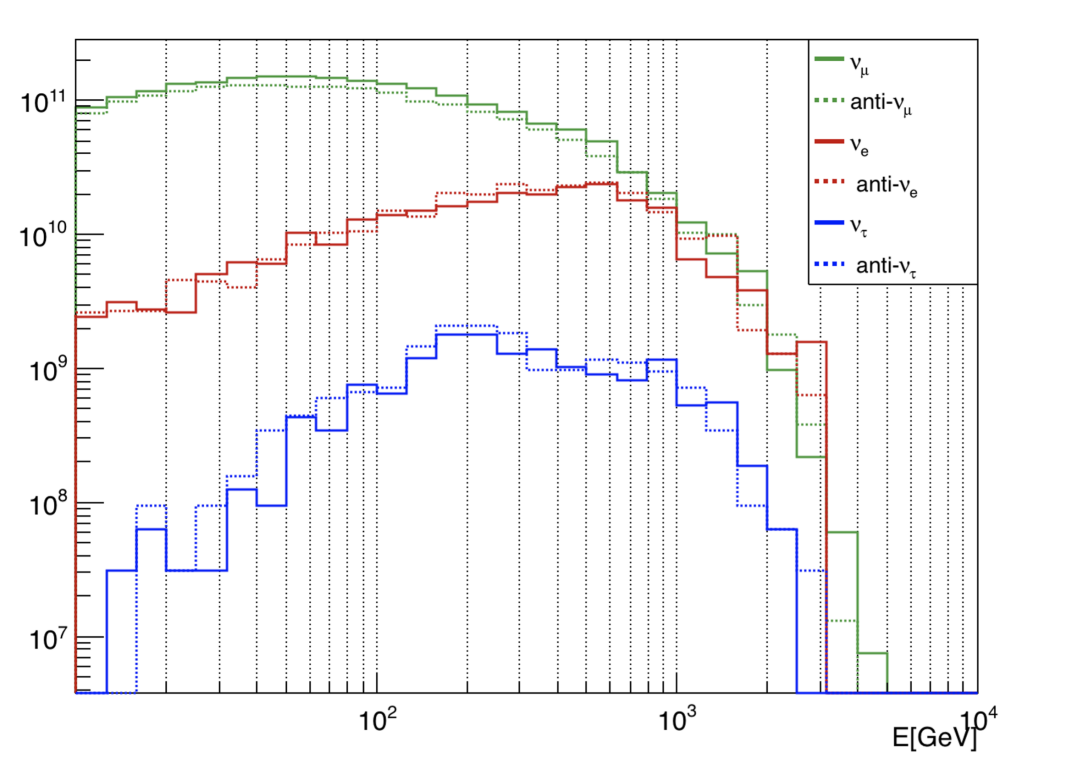

Figure 2.3: Energy values of incoming νs and $\bar{\nu}$s predicted by the DPMJET/FLUKA simulation. The normalization corresponds to 250 fb^{-1} [9].

cays' contribution at IP1 to be around 3%. Assuming that the deep-inelastic charged-current cross-section of the electron neutrinos follows the SM prediction, electron neutrinos can be used as a probe of charm production in the pseudo-rapidity range of SND@LHC after unfolding the instrumental effects and subtracting the K contribution. The energy spectrum of the incoming electron-neutrino flux is estimated by a method that starts with the energy spectrum of the electron-neutrino and then unfolds the effects of energy resolution. At that point, data can be used to measure the pp $\rightarrow$ ν_eX cross-section with an accuracy of 15%, where the primary source of the error is systematic uncertainty of the unfolding process [2].

Even though different event generators produce different amounts of kaon contribution, they all agree that the events are limited to energies below 200 GeV. The uncertainty in the production of kaon results in additional 20% uncertainty in the production of heavy-quark when the kaon contribution is subtracted [2].

A two-step analysis is used to determine the yield of charmed hadrons producing neutrinos in the SND@LHC pseudo-rapidity range: first, measuring the pp $\rightarrow$ ν_eX cross-section, and second, deriving the charmed-hadron yield from the electron neutrino flux. A comprehensive method with a full simulation has been set up to correlate the yield of charmed hadrons in a given η region with the neutrinos in the measured η region, which leads to an additional 25% systematic uncertainty in the charmed-hadron yield [2]. The measurement of the charmed-hadron production in pp collision can, therefore, be performed with a statistical uncertainty of approximately 5%, with the systematic error accounting for the majority of the uncertainty at 35% [2].

Parton distribution functions (PDF) represent the probability of finding a parton (quark and gluon) in a hadron as a function of the x, where x is the ratio of the parton momentum to the hadron momentum, bjorken-x [11]. PDF gives details about the gluonic structure of nucleons. Measurement of charmed hadron production in deep inelastic scatterings is important since pairs of charm quarks are produced with photon-gluon fusion, as illustrated in Figure 2.4. Information on the gluon parton distribution function in an untouched longitudinal momentum fraction (x) region can also be obtained from there.

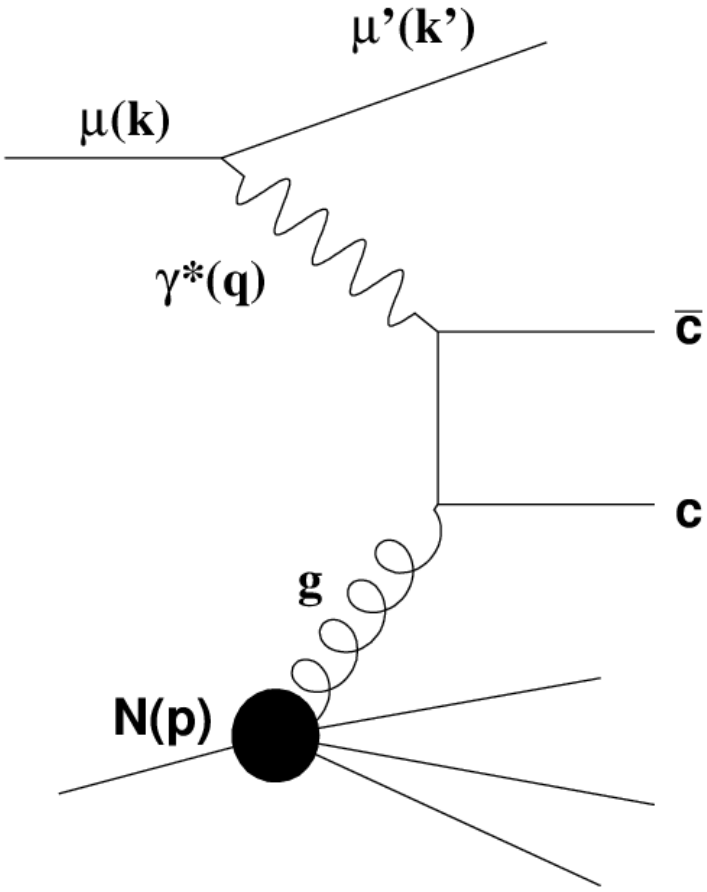

Figure 2.4: The photon-gluon fusion process in charm and anti-charm pair production. Symbols in parentheses represent four-vectors. Retrieved from Leading and Next-to-Leading Order Gluon Polarisation in the Nucleon and Longitudinal Double Spin Asymmetries from Open Charm Muoproduction.

2.2 Lepton Flavour Universality test in ν interactions

Lepton Flavour Universality states that all three charged types of leptons should exhibit the same behavior in specific interactions involving the weak nuclear force. In other words, electrons, muons, and taus should all be treated equivalently by the weak nuclear force, one of the fundamental natural forces governing processes like radioactive decay. The weak force should interact with leptons in the same way regardless of their generation. According to the Standard Model of particle physics, electrons, muons, and taus should all experience the weak force similarly. To test this, it is necessary to study the interactions of different neutrino flavours.

The concept of Lepton Flavour Universality is crucial for several reasons, including precision SM testing, investigating new physics, implications for cosmology, and verifying the SM. Various experiments have tested Lepton Flavour Universality, including heavy meson and tau lepton decays. The successful demonstration of Lepton Flavour Universality lends support to the SM.

The ability of the SND@LHC detector to distinguish all three types of neutrino flavours provides a unique opportunity for testing Lepton Flavour Universality in neutrino interactions [2]. The positioning of the SND@LHC detector makes it possible to observe the neutrino flux resulting from the decays of the c and b quarks, opening access to tau neutrinos via the decays of D_s mesons. Figure 2.5 shows the muon and electron neutrino spectra in the SND@LHC acceptance region, with the component resulting from heavy-quark decays represented by the filled area.

In the pseudo-rapidity range of SND@LHC, tau neutrinos are essentially produced in the decay of D_s mesons ($D_s \rightarrow \tau\ \nu_\tau$) and the subsequent τ decays. According to the Pythia event generator, approximately 8% of ν_τs comes from beauty hadron decays [2]. The ν_e to ν_τ ratio depends only on the decay branching ratios and the charm hadronization fractions, assuming that both tau and electron neutrinos come from the decay of charmed hadrons. The ratio becomes sensitive to the cross-section ratio of the two neutrino species as the systematic uncertainties resulting from the charm-quark production mechanism cancel out. Thus, the measurement of this ratio can be viewed as a Lepton Flavour Universality test in neutrino interactions. The

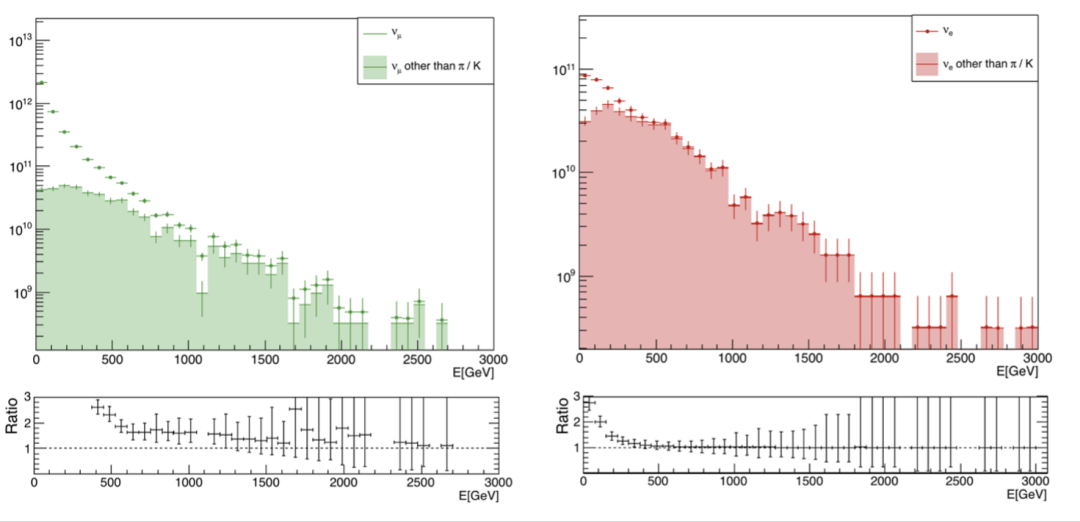

Figure 2.5: Muon and electron neutrino energy spectra in the SND@LHC acceptance region [2].

known branching ratios and the charmed hadron species in acceptance can be used to express the ν_e/ν_τ ratio. The statistical uncertainty is dominated by the low statistics of the ν_τ sample, corresponding to a 30% accuracy. Compared, weighted branching ratio estimations are influenced by a systematic uncertainty of approximately 22% [2].

The ν_e/ν_μ ratio can be used as a Lepton Flavour Universality test in neutrino interactions. Compared to ν_τs, the scenario is somewhat different for ν_μs. The production mechanism cannot be considered the same as in the case of ν_e because the ν_μs are considerably more abundant but extensively contaminated by π and K decays. However, the majority of this contamination concentrates at low energies. The contamination is predicted to decrease to approximately 35% and remains stable for energy above 600 GeV [2]. Furthermore, charmed hadron decays have approximately equivalent branching ratios into ν_es and ν_μs. As a result, the systematic uncertainties in the weighted branching fractions do not affect the ν_e/ν_μ ratio. Two systematic uncertainties, one resulting from the π and K production in this pseudo-rapidity range and the other from their propagation through the machine components along the beamline, have an impact on the yield of ν_μs from π and K decays. The measurements available used to confine the simulation allow for an evaluation of both contributions. As a result, the ν_e/ν_μ ratio provides a test of the Lepton Flavour Universality with a 15%

uncertainty, with an equal 10% statistical and systematic contribution [2]. It should be emphasized that SND@LHC measures the particle flux in TI18 and perhaps in other locations along the beamline with high accuracy, helping to compare the tools for particle propagation and decreasing systematic uncertainties.

2.3 Measurement of the NC/CC ratio

Deep inelastic scattering (DIS) is a process used to probe the insides of hadrons (particularly the baryons, such as protons and neutrons) using electrons, muons, and neutrinos. It is by far a significant amount of predominating interaction mechanism at the high energy of the LHC neutrinos. In CC interaction, a charged lepton changes its corresponding neutrino, the same for antiparticles. In NC interaction, the same particle goes in and out; particle identity does not change.

The NC/CC ratio measurement is important since it can be used as an internal consistency test [5][6]. Identification of the charged leptons associated with the three flavours is necessary to distinguish between NC and CC interactions. However, in the absence of a magnetic field, charge identification is not possible. Then, the CC interactions with νs and $\bar{\nu}$s cannot be distinguished. Also, distinguishing the flavours of NC interactions is not possible [9]. The ratio of the NC/CC cross-section is equal to the ratio of the observed events under the assumption that the differential neutrino and anti-neutrino fluxes are equal:

$$P = \frac{\sum_i \sigma_{NC}^{\nu_i} + \sigma_{NC}^{\bar{\nu}_i}}{\sum_i \sigma_{CC}^{\nu_i} + \sigma_{CC}^{\bar{\nu}_i}} \tag{2.1}$$

The NC/CC deep-inelastic interaction cross-section ratio at a given energy may be expressed in terms of the Weinberg angle and a correction factor related to the non-isoscalarity of the target material [2]:

$$P = \frac{1}{2}\left\{1 - 2\sin^2\theta_W + \frac{20}{9}\sin^4\theta_W - \lambda(1 - 2\sin^2\theta_W)\sin^2\theta_W\right\} \tag{2.2}$$

where θ_W is the Weinberg angle, which is related to the probability that a neutrino

would interact with matter, resulting in a scattered neutrino and the remains of the target, and the λ is the correction factor related to the target material. The Weinberg angle, also known as the weak mixing angle, is one of the fundamental parameters of the standard model of elementary particles, that has been accurately measured [14]. The non-isoscalarity of the target material introduces a correction factor indicated by λ, which is estimated to be 0.04 for tungsten. This correction factor is crucial for the cross-section ratio to be measured accurately.

2.4 Neutrino-induced charm production

The production and behavior of charm quarks give the opportunity to test the Standard Model's predictions of particle physics. Any deviations from these predictions could point to a new physics beyond the Standard Model.

High-energy neutrino interactions are an effective instrument for studying the physics of charms since they can produce charmed hadrons [2]. Charm hadron production in neutrino and anti-neutrino interactions are illustrated in the Feynman diagrams in Figure 2.6.

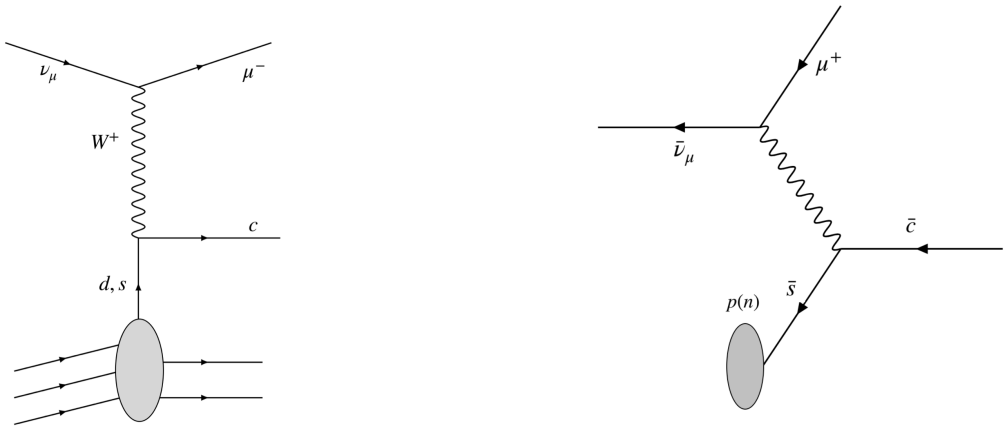

Figure 2.6: Feynman diagrams for neutrino (left) and anti-neutrino (right) CC interactions. Time runs from left to right. Particles are shown by positive time direction arrows, whereas antiparticles are indicated by negative time direction arrows [2].

The use of nuclear emulsions provides a unique opportunity to identify charmed

hadrons by observing a two-vertex topology. The NuTeV experiment observed 5102 charmed hadron candidates in muon neutrino CC interactions and 1458 in muon anti-neutrino CC interactions [2]. The emulsion experiment CHORUS observed 2013 charmed hadron candidates from muon neutrinos and 32 from muon anti-neutrinos. A tau-neutrino candidate with charmed-hadron production was also observed by the OPERA experiment. There has never been a report of an electron-neutrino interaction with a charm candidate.

In summary, as shown in Table 2.1, in the analyses of neutrino interactions, the measurements of

- pp $\rightarrow \nu_e$X cross-section has 5% statistical and 15% systematic uncertainty,
- charmed hadron production in pp collisions has 5% statistical and 35% systematic uncertainty,
- ν_e/ν_τ ratio for LFU test has 30% statistical and 22% systematic uncertainty,
- ν_e/ν_μ ratio for LFU test has 10% statistical and 10% systematic uncertainty, and
- NC/CC ratio has 5% statistical and 10% systematic uncertainty [2].

Table 2.1: Proposed measurements and uncertainties by the SND@LHC in the analyses of neutrino interactions.

Measurement	Statistical	Systematic
pp $\rightarrow \nu_e$X cross-section	5%	15%
Charmed hadron production	5%	35%
ν_e/ν_τ ratio for LFU test	30%	22%
ν_e/ν_μ ratio for LFU test	10%	10%
NC/CC ratio	5%	10%

CHAPTER 3

DETECTOR LAYOUT

The SND@LHC detector is a hybrid system made up of different components that have been designed to detect neutrino interactions effectively. It contains an 830 kg target section comprised of tungsten plates located between nuclear emulsions and electronic trackers [2][12]. The detector includes a muon system and a hadronic calorimeter as essential components. In order to tag muons, measure electromagnetic and hadronic energy, and preselect the interaction zone, electronic detectors are crucial. On the other hand, the emulsion detectors provide excellent vertex reconstruction capabilities, improving the accuracy of particle tracking. The detector operates a right-handed coordinate system, with x pointing away from the LHC's center, z aligned with the nominal collision axis, and y pointing upward and vertically aligned. SND@LHC uses an off-axis setup. The positioning of the SND@LHC detector in the TI18 tunnel is shown in Figure 3.1, and in Figure 3.2, the detector layout is represented in detail. An actual photo of the detector is also shown in Figure 3.3.

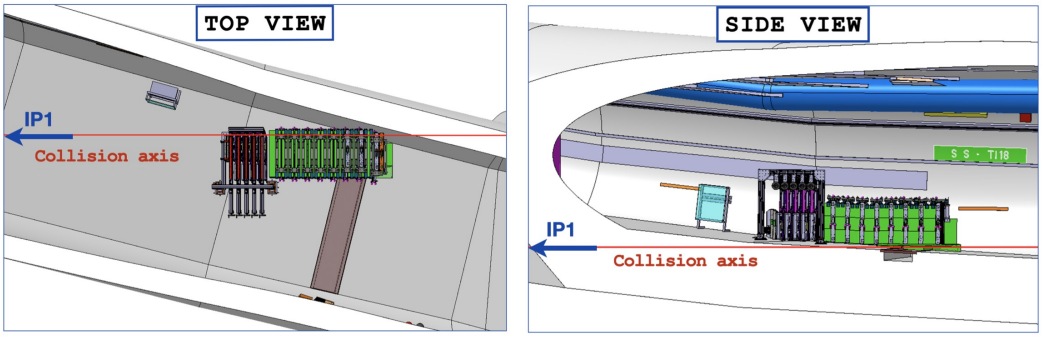

Figure 3.1: SND@LHC detector in the TI18 tunnel [12].

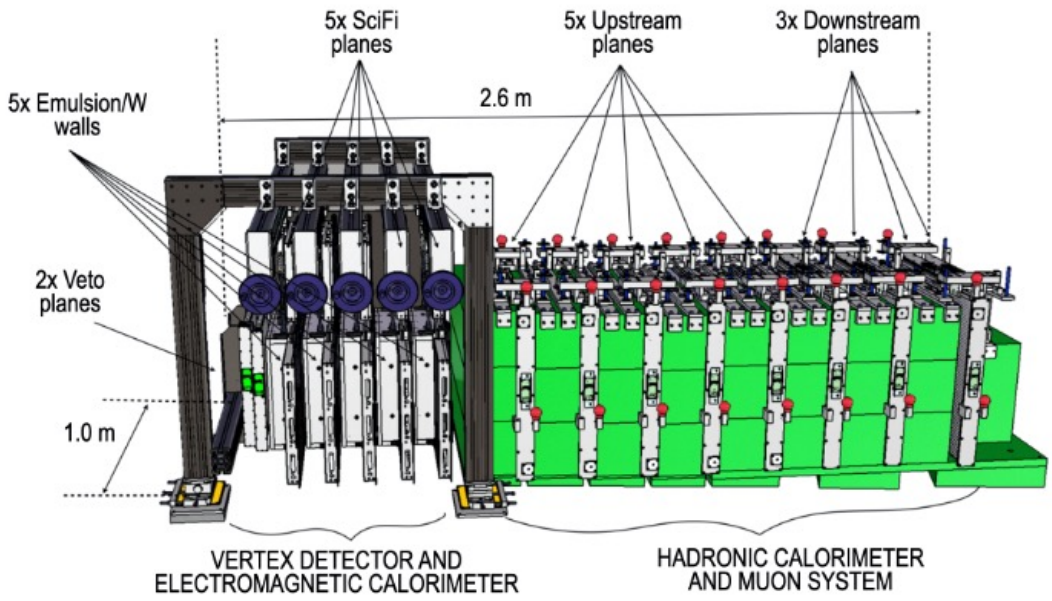

Figure 3.2: SND@LHC detector layout [9].

The detector is divided into three sections: the upstream veto system, the five-walled target section, and the hadronic calorimeter and muon system. The purpose of the veto system is to reject charged particles, especially muons incoming from the IP1 direction, using scintillating bars read out by silicon photomultipliers (SiPMs). The target tracker system consists of 5 SciFi (scintillating fiber) planes and a target region. SciFi trackers provide timestamps for the neutrino interactions reconstructed in the ECC walls in the target region and also energy measurement of electromagnetic showers. Additionally, SciFi serves as a hadronic calorimeter with the scintillating bars in the muon system. They provide energy measurement of the hadronic jet produced in the neutrino interaction and, thus, of neutrinos. The alternating x and y views of the scintillating fiber stations provide spatial resolutions of about 150 μm and time resolutions of about 250 ps for particle interactions [2]. The muon system identifies muons, which is crucial to identifying muon neutrino charged-current interactions. Scintillating planes in the muon system provide fast time resolution and energy measurement. The muon system and hadronic calorimeter consist of upstream and downstream parts equipped with scintillator bars interleaved with iron blocks. The downstream part provides better spatial resolution, enabling the identification of muon tracks exiting the detector. The target section, essential for tracking charged particles created in high-energy neutrino interactions, comprises scintillating

Figure 3.3: A picture of the SND©LHC detector, with an average-sized person for size comparison.

fiber stations for tracking and electromagnetic calorimetry and emulsion cloud chambers (ECC). The submicrometric spatial resolution of the nuclear emulsions provides effective particle tracking. This is essential for identifying tau leptons and tagging tau neutrino interactions. Each ECC unit consists of a series of 60 (or 57) nuclear emulsion films interleaved with tungsten plates, resulting in a target mass of around 830 kg.

The extensive design and advanced components of the SND@LHC detector offer a crucial basis for accurate neutrino interaction measurements while opening the way to revolutionary research regarding high-energy neutrino physics. In accordance with the focus of this thesis work, the SND@LHC target and vertex detector will be dis-

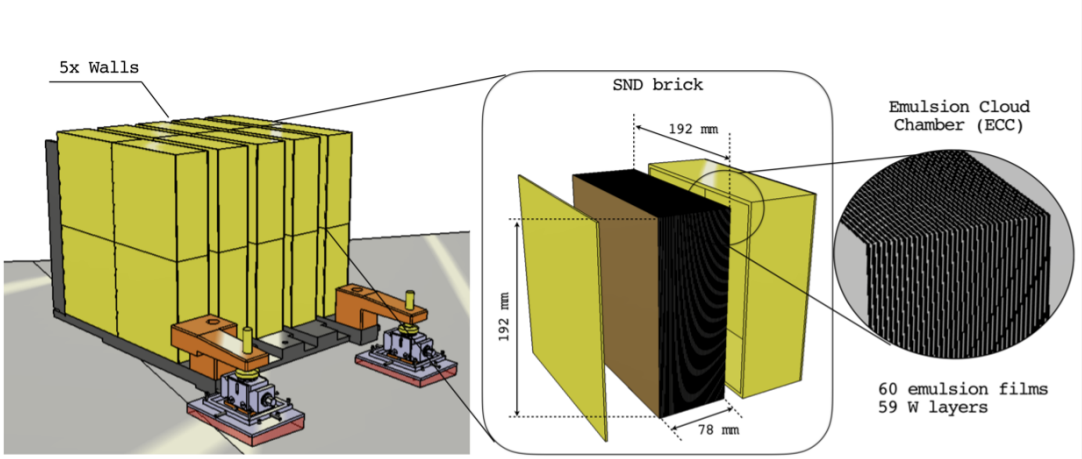

Figure 3.4: Schematic view of the SND@LHC emulsion target and the ECC [2].

cussed in detail in Section 3.1.

3.1 Target and vertex detector

The emulsion target of the SND@LHC detector consists of five walls, each consisting of four unitary cells called "brick." Emulsion films are placed in these bricks with interleaving tungsten plates. Each brick consists of 57 Nagoya (N) or 60 Slavich (S) films and 56 or 59 tungsten plates, respectively. That is, the detector contains about 1200 emulsion films, for a total of 44 m^2. This setup is built following the Emulsion Cloud Chamber (ECC) technique, as illustrated in Figure 3.4.

Combining nuclear emulsion films interleaved with tungsten layers, the ECC technology provides a tracking device with a sub-micrometric position and milliradian angular resolution [2]. The ECC technology can identify leptons and charmed hadrons by distinguishing their production and decay vertices. It is also suitable for FIP detection by direct observation of scattering off electrons or nucleons in the tungsten plates. The remarkable spatial resolution of nuclear emulsion films enables electron identification by detecting electromagnetic showers in the brick.

Emulsion films are labeled before they are placed in bricks. Figure 3.5 shows an emulsion film and its label. An emulsion label is written to indicate the run number,

the wall number, the brick number, the plate number, and the film manufacturer in order.

3.1.1 Target Walls

3.1.1.1 Emulsion films

Nuclear emulsion films are preferred in tracking detectors because they provide sub-micrometric position and milliradian angular resolution. Also, they are the most compact, thinnest, and lightest three-dimensional tracking detectors.

Nuclear emulsion films are made up of silver bromide (AgBr) crystals distributed in a gelatin binder. AgBr crystals, with a 0.2 μm diameter, respond to minimum ionizing particles (MIP). When a MIP passes through, a series of activated AgBr crystals create a latent image, effectively tracing the trajectory of the particle. Latent pictures are made more intense with a chemical process known as development, leading to the growth of silver clusters (grains) with a diameter of 0.6 μm that can be seen under an optical microscope.

A nuclear emulsion film is made up of two sensitive layers, each 70 micrometers thick, placed on either side of a transparent plastic that is 170 micrometers thick. Connecting the two hits left by a charged particle on opposite sides of the base allows milliradian-level precision in measuring the track's slope. Figure 3.6 represents a cross-sectional view of the emulsion film and an image of an interaction vertex within the plastic base as visible by an optical microscope.

Emulsion films used in SND@LHC have a size of 192 x 192 mm^2 and are produced by Nagoya University in Japan and by the Slavich Company in Russia.

3.1.1.2 Tungsten target

The interaction rate per unit volume is maximized by choosing tungsten as the target material. Additionally, it enables successful electromagnetic shower reconstruction in the ECC. For use in emulsion detectors, tungsten is a good material due to its low

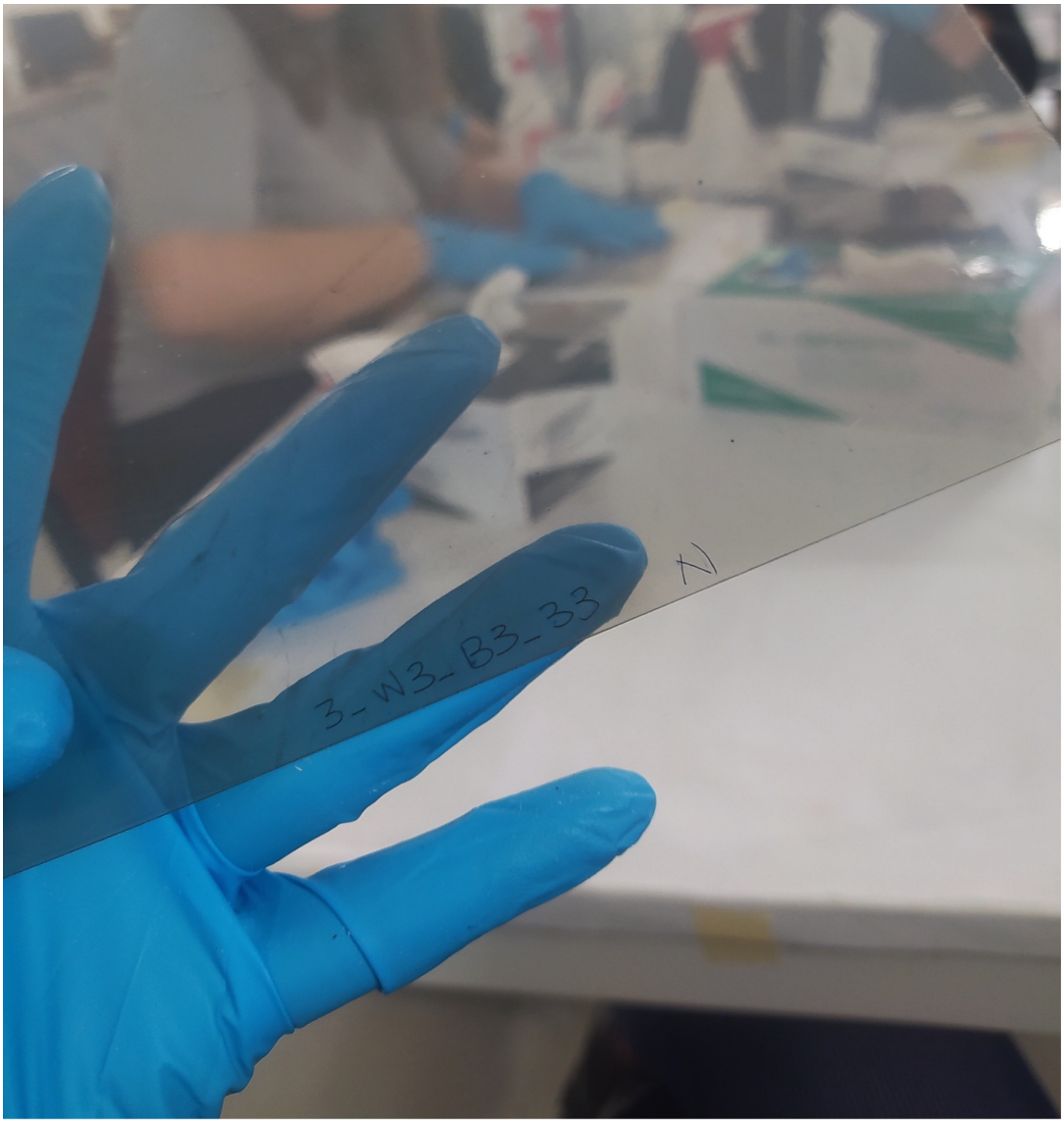

Figure 3.5: An emulsion with its label (3-W3-B3-33 N). "3" indicates RUN3, "W3" indicates Wall 3, "B3" indicates the third brick, "33" indicates the plate number, and "N" indicates that it is produced in Nagoya, respectively.

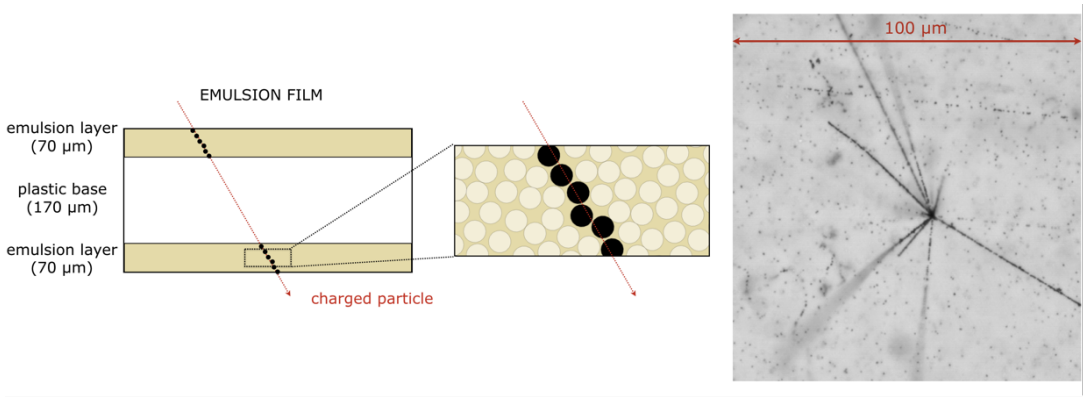

Figure 3.6: Cross-sectional view of an emulsion film (left). The red lines represent the trajectory of a charged particle. View of a film under the optical microscope (Right). Some nuclear fragments emitting from the interaction vertex are seen [2].

intrinsic radioactivity. 192 x 192 mm^2 tungsten plates are placed between emulsion films in each brick of the 5 walls.

3.1.1.3 Chemical development

The development is a procedure that uses chemical amplification to make the latent image in the emulsion film visible under the optical microscope. There are five steps for it:

- Development: transforming a cluster of a few silver atoms into a visible metallic silver grain
- Stop: to end the development process instantly
- Fix: dissolving any remaining silver halide crystals, leaving the metallic silver that forms the image
- Wash: removing all silver thiosulphate complexes from the emulsion
- Thickening: making the emulsion back to its original thickness

Figure 3.7 shows a picture of the tanks while the chemical compounds for the development are being prepared. The development process takes place in a dark room.

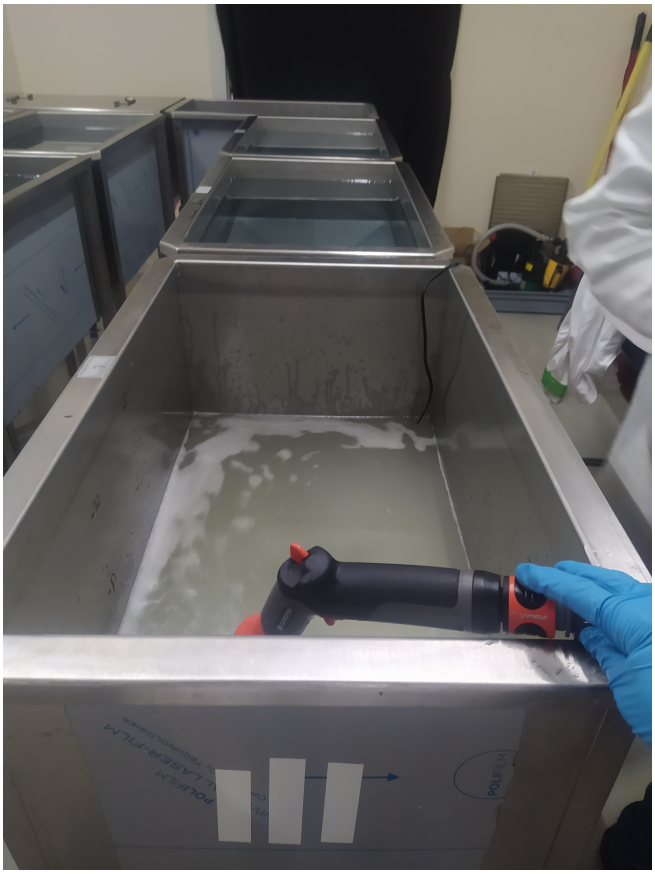

Figure 3.7: A picture of the tanks being filled with chemical compounds for the development of the emulsion films.

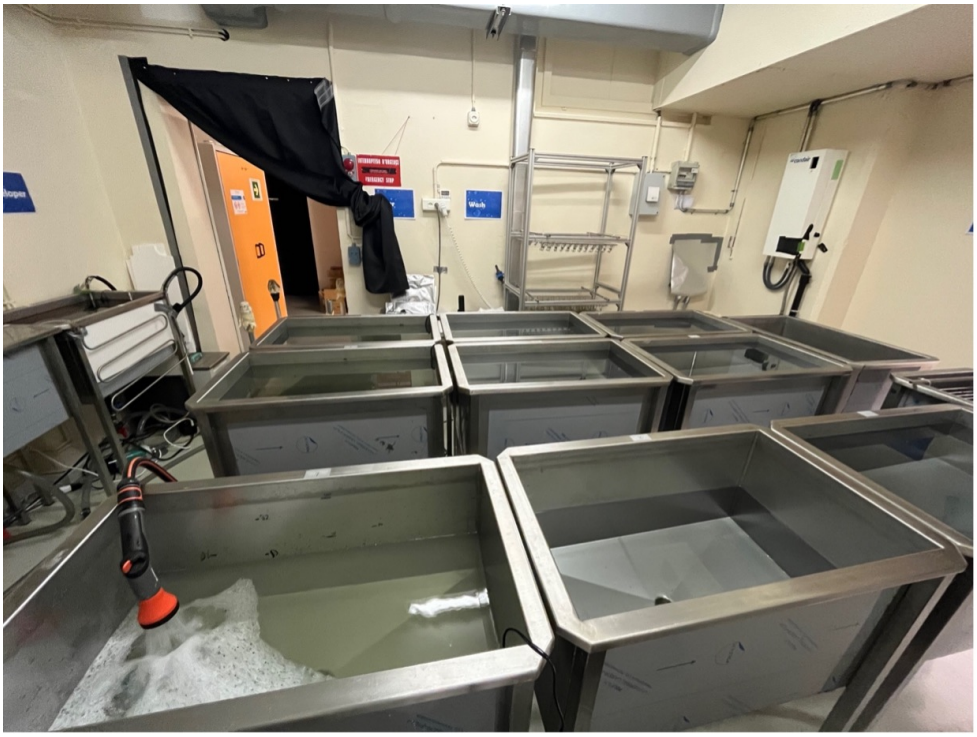

Figure 3.8: The dark room at CERN where the development process takes place.

Figure 3.8 shows a picture of the dark room where the chemical treatment of emulsion films is performed at CERN. After this process, emulsion films are ready for scanning, which will be mentioned in section 4.2. The emulsion films are then packed and sent to scanning stations —a photograph while packaging is shown in Figure 3.9.

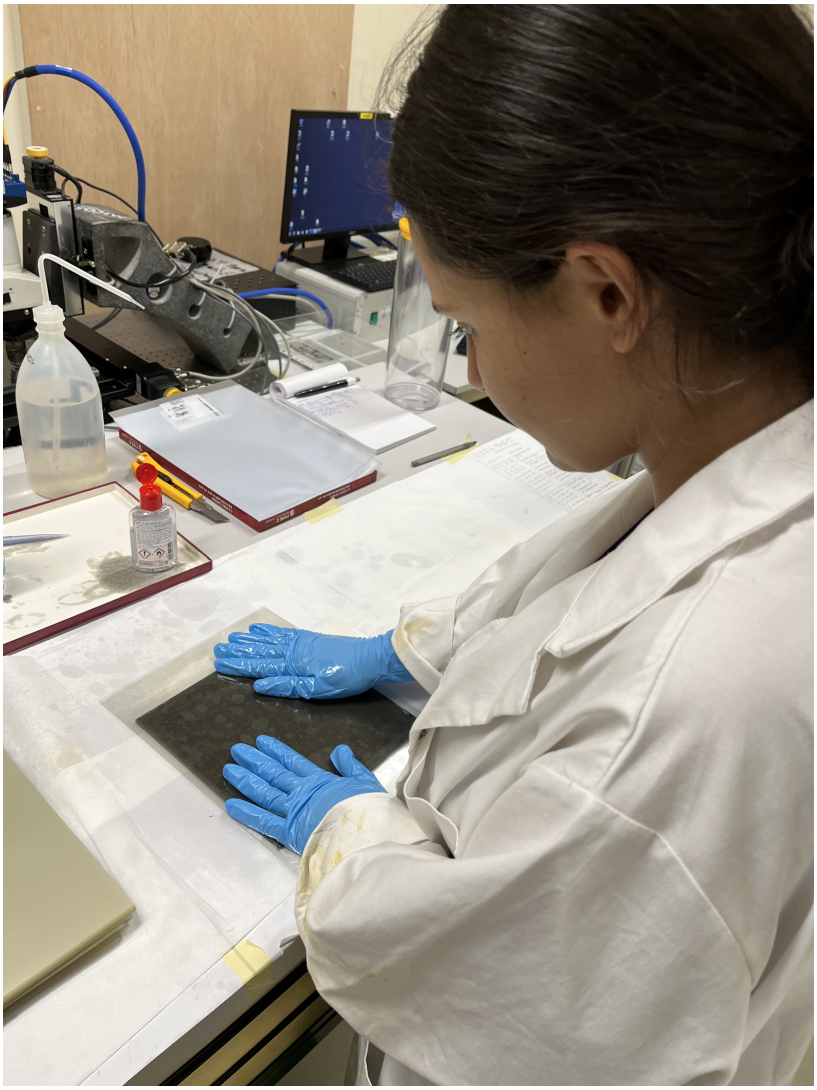

Figure 3.9: A photo while packaging at CERN Emulsion Facility.

CHAPTER 4

DATA RECONSTRUCTION

The SND@LHC detector was installed during Long Shutdown 2 in 2021 and started to operate during the LHC Run 3 [9]. The first LHC Run 3 stable beams were delivered in July 2022 at a center-of-mass energy of 13.6 TeV. The emulsion target replacements are named "Emulsion RUNs". This chapter will focus on the reconstruction and the analysis of Emulsion RUN0 data, which has collected integrated luminosity of 0.52 fb^{-1}.

Raw data is archived on tape, and raw and reconstructed data is available on EOS (The CERN Disk Storage System) for analysis.

The event reconstruction is done in two stages; the first uses the electronic detectors' response during data taking. The second one is the reconstruction of the emulsion data, available after the extraction, development, and scanning processes and reconstruction of the emulsion data.

4.1 SND@LHC Software

The software framework for SND@LHC, sndsw, is developed for effective offline data analysis. To improve accessibility and visibility, display tools that are used in detector commissioning have been improved throughout time. In the framework, various simulation engines are used [2]. Some of them can be listed as follows:

- FLUKA: for simulation of muons from IP1
- Geant4: for detector interactions

- Pythia6, DPMJET3, Pythia8: simulation of muon deep inelastic scattering and neutrino production at IP1

- GENIE: for simulation of neutrino interactions in the detector target

4.2 Emulsion Scanning

The emulsion scanning is carried out in specialized laboratories using automated optical microscopes. One of the optical microscopes is shown in Figure 4.1. The microscopes' hardware and software have constantly improved.

The European Scanning System (ESS) has been updated, combining a faster camera with smaller sensor pixels and a higher number of pixels [2]. Additionally, new software LASSO and a lower-magnification objective lens have been used. The combination of these improvements provides a higher scanning speed of $180 cm^2$/h, increasing the previous rate by a factor of more than ten. The lens of the optical microscope provides resolution at sub-micron and allows the scan of both surfaces of the emulsion film. An immersion lens in oil with the same refractive index as the emulsion is used to maintain uniformity in the optical path through the film. A single field of view is 800x600 μm^2. To scan larger regions, scanning is done by data acquisition across a grid of neighboring fields of view, choosing the bottom-left corner of the emulsion film as the starting point (xy origin). To reduce noise, the images captured by the digital camera are transferred to a vision processing board in the control workstation.

SND@LHC emulsion films are undergoing scanning across several scanning stations in Europe: two microscopes are situated in Naples, one in Bologna, another in Lebedev, and four in the CERN emulsion facility. The scanning and processing of RUN0 have already been done in Naples. Films from other emulsion RUNs have been shared among all the participating laboratories. A close-up photograph of the optical microscope at the CERN emulsion facility is shown in Figure 4.2.

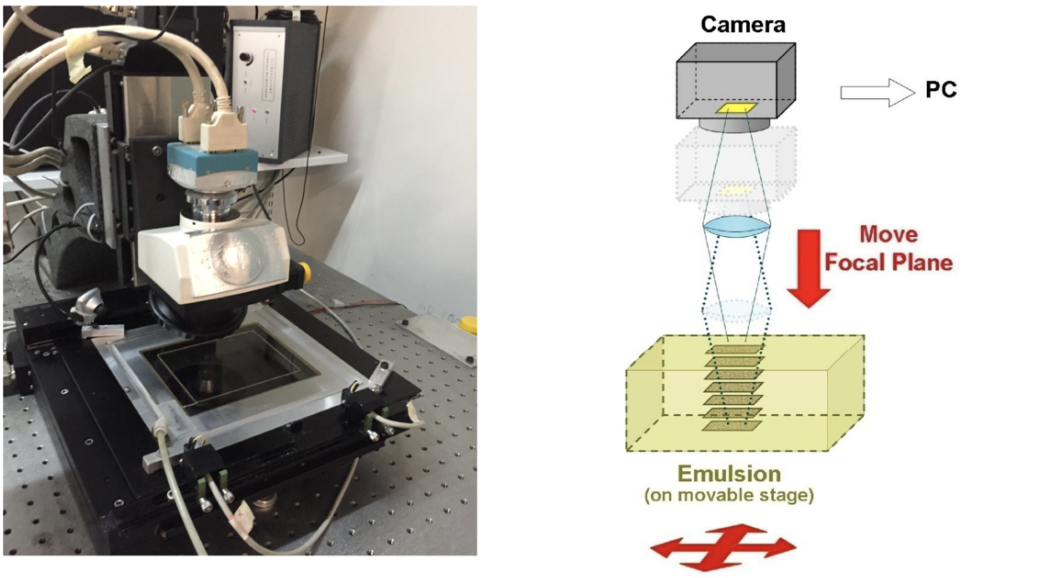

Figure 4.1: Optical microscope used in emulsion scanning (left). Diagram illustrating the scanning process (right) [2].

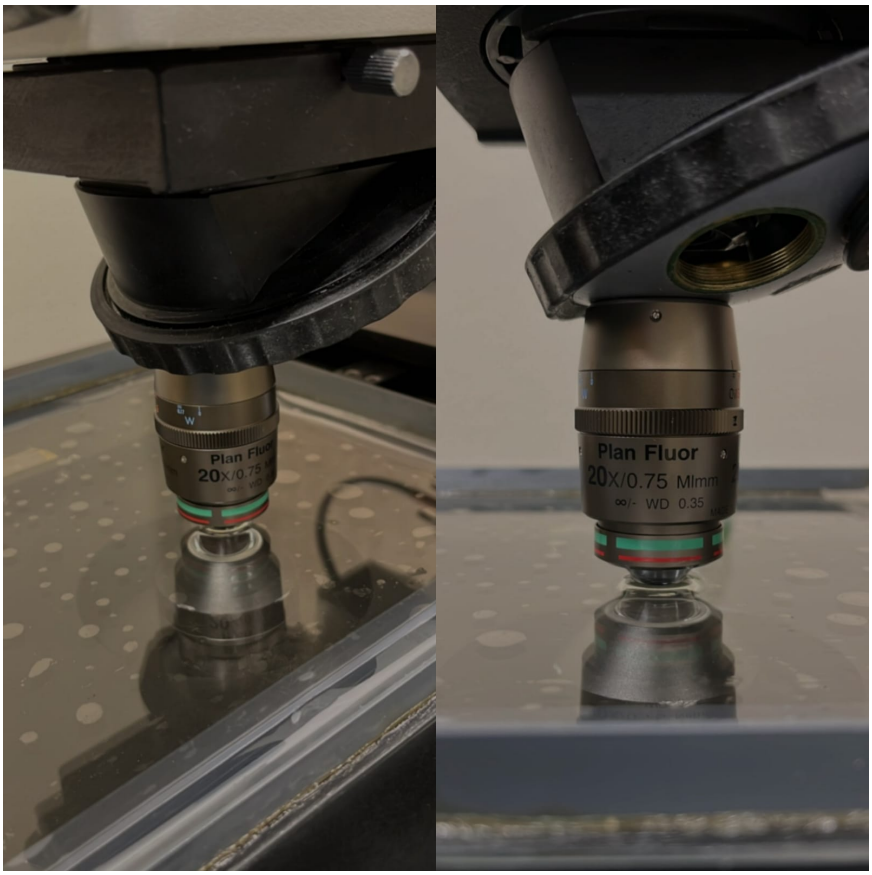

Figure 4.2: a close-up photograph of the optical microscope during the scanning.

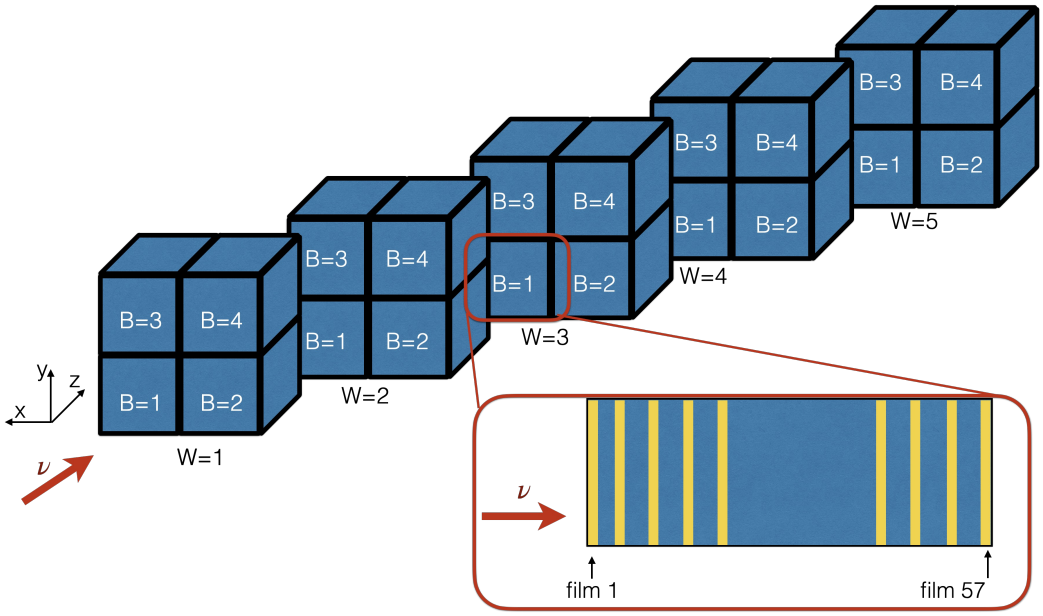

Figure 4.3: Schematic view of the SND@LHC target. The brick full of emulsions for RUN0 is shown with the red box. Retrieved from "Study of neutrino interactions at SND@LHC," Alicante, F., 2023.

4.3 Emulsion RUN0 Reconstruction

The initial months following detector installation have been characterized by low integrated luminosity during beam commissioning and scrubbing. Therefore, from April 7 to July 26, 2022, only one out of twenty bricks was instrumented with 57 emulsion films. The remaining bricks were filled only with tungsten plates for the optimization of the usage of emulsion films. Figure 4.3 displays the "Emulsion RUN0" layout for this setup. The integrated luminosity is 0.52 fb^{-1}. This choice was made to determine the quality of the data reconstruction process, from emulsion scanning to all reconstruction processes. In the following sections, the procedure of the linking, alignment, tracking, and vertexing algorithms and their results for RUN0 will be discussed.

4.3.1 Linking

The microscope scans the whole thickness of the emulsion and obtains tomographic images at equally spaced depths. Obtained images are digitized, and the image pro-

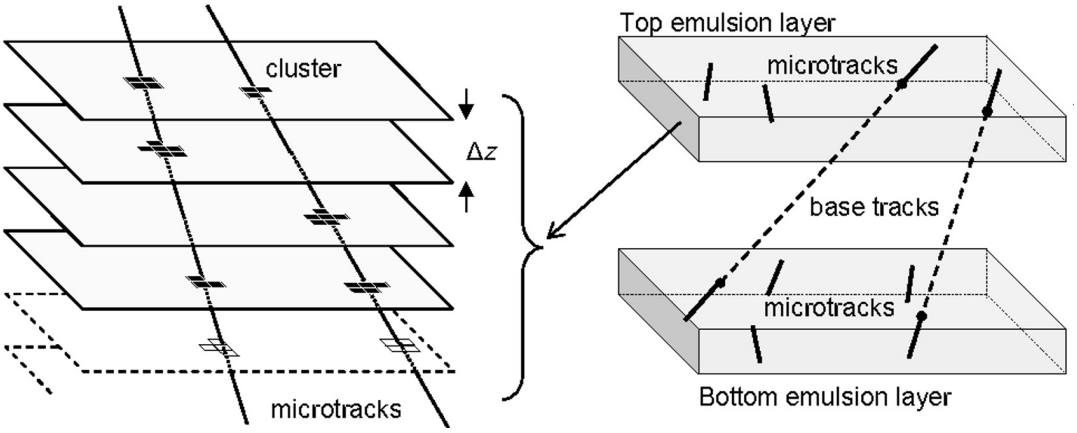

Figure 4.4: A schematic representation of reconstruction of micro-tracks (left) and base-tracks (right). Retrieved from “Nuclear Emulsions,” Ariga A., Ariga T., Lellis G., Ereditato A., and Niwa K., 2020.

cessor defines the grains as "clusters", which are collections of pixels with specific sizes and shapes. Then, the "micro-track" in the emulsion layer is created by linking clusters in the different levels, as illustrated in Figure 4.4 (left). As an emulsion film has two layers, connecting the two micro-tracks through the plastic base results in the reconstruction of the particle’s path within the emulsion film, known as a "base-track" (segment), as illustrated in Figure 4.4 (right).

The linking procedure for the emulsion data is a critical stage in the reconstruction process, and it involves constructing particle tracks using the information obtained during the scanning of the emulsion films. A description of the linking process is provided below:

1. Cluster Recognition: The first step in the procedure is to digitize the images obtained from the scanned emulsion films. An image processor recognizes clusters, which are collections of neighboring pixels with similar characteristics, such as intensity or color. These clusters correspond to grain positions in emulsion films created by particle interactions.

2. Micro-Tracks: Each cluster in the emulsion layer indicates a particular particle interaction. The term "micro-track" refers to the connection of clusters from different levels of the emulsion layer. A micro-track is a representation of the

path of a particle through the emulsion layer.

3. Base-Tracks: Because emulsion films have two layers, connecting the micro-tracks in the two layers is necessary to form a "base-track" (segment). The base-track represents a particle's path through a single film. The information from the two layers is combined throughout this procedure to provide a complete image of the particle's path through the film.

4. FEDRA Reconstruction Tools: The offline reconstruction tools used in this procedure are part of the FEDRA (Framework for Emulsion Data Reconstruction and Analysis) software [1]. FEDRA is a software developed in C++ within the ROOT framework that offers an infrastructure for handling and processing emulsion data.

5. First-linking and Shrinkage Correction: There are two phases in the linking process. The first phase, known as "first-linking," is to evaluate shrinkage and apply angular corrections to the micro-tracks. Shrinkage is the reduction in emulsion size caused by processing. To improve the accuracy of the tracks, these corrections are calculated.

6. Base-Track Selection: In the second phase of linking, base-tracks are selected using a χ^2 minimization process. To find the most suitable match for the particle's path, this process involves considering a variety of parameters as input, such as coordinates, angles, and cluster numbers. The chosen base-tracks illustrate the most likely trajectories of the particles through the emulsion film.

7. Uniform Base-Track Density: The emulsion films in the same brick have a consistent distribution of base-tracks across their surface. This uniformity is crucial because it contributes to creating a reliable frame of reference for tracking and reconstruction.

8. Reference Angles: The components of the base-tracks in the xz (TX) and yz (TY) planes are used to determine the angles of the base-tracks (θ_x and θ_y). These angles give details about the direction and orientation of the particle's path through the emulsion film. The coordinate system is illustrated in Figure 4.3.

In summary, the linking process in the reconstruction of emulsion data includes building micro-tracks from clusters, connecting micro-tracks from different emulsion layers to generate base-tracks, and choosing the best base-tracks based on minimizing χ^2 values. This procedure is crucial for the accurate reconstruction of particle trajectories within emulsion films and is supported by the FEDRA software framework.

4.3.2 Alignment

4.3.2.1 Global Alignment

Reconstructing particle tracks throughout the entire volume involves linking base-tracks identified in consecutive emulsion films. In order to define a global reference system, a series of transformations need to be calculated to accommodate the distinct coordinate systems used for data obtained in different films. The penetrating muon tracks from the IP1 are used to make fine film-to-film alignment. Reconstructing volume-tracks, charged tracks that cross multiple emulsion films, becomes possible if alignment is determined across all emulsion films. Global alignment guarantees that the locations and orientations of particle tracks recorded in different films are accurately connected, allowing for the reconstruction of particle trajectories crossing multiple films. It provides a single global reference frame, allowing complete track reconstruction and analysis. Global alignment steps can be explained as follows:

1. The first step is determining the positions and orientations of particle tracks or clusters in the emulsion film's own coordinate system. Each film has its own local reference frame. This coordinate system's z-axis is located at the center of the emulsion film.

2. As a second step, pairwise alignment starts. Within the brick, pairs of consecutive emulsion films are aligned with each other. In order to do this, the orientations and locations of one film in relation to the other must be adjusted. In order to minimize differences between the emulsion films, transformations are used to account for translations, rotations, and other adjustments.

3. Global Reference System: A global reference system is created by iteratively

applying pairwise alignment to all consecutive pairs of films in the brick. All of the films in the brick have a common framework due to this reference system, which guarantees that all emulsion films in the brick are appropriately aligned with respect to each other.

4. Consistency Checks: Following the application of the global alignment, consistency checks are done to ensure the accuracy of the alignment process. These tests include analyzing the particle tracks' continuity between films. Any inconsistencies or misalignments can be found and corrected.

To summarize, the global alignment procedure for the emulsion films in the brick involves aligning one film with regard to the others, resulting in a single reference frame that allows for the accurate reconstruction of particle tracks over multiple emulsion films. By ensuring that the data from various films are calibrated and positioned correctly, this procedure makes it easier to analyze particle interactions and trajectories inside the experimental setup.

The analyzed data in this thesis work consists of 31 consecutive emulsion films. The position and angular resolutions of each "long track" are checked. For the choice of long tracks, tracks with the number of segments larger than 20 were chosen. The tracking resolution is calculated by computing the residuals between the position and angle of each base-track with a linear fit on the xz and yz planes. To calculate the resolution, the distance of each segment of a track to the linear fit of the track, which is named "position residual", is calculated for both x and y positions. Also, for the "angular residual", the difference between the angle of each track segment and the linear fit angle is calculated for both θ_x and θ_y. These calculations iterate over all tracks, then position and angular resolution histograms are obtained, and a Gaussian fit is applied to the distributions as shown in Figure 4.5 and 4.6.

4.3.2.2 Local Alignment

Local alignment of an emulsion film refers to determining the locations and orientations of clusters within that specific film's coordinate system. This entails locating cluster centroids (center points) and calculating their angles relative to a predeter-

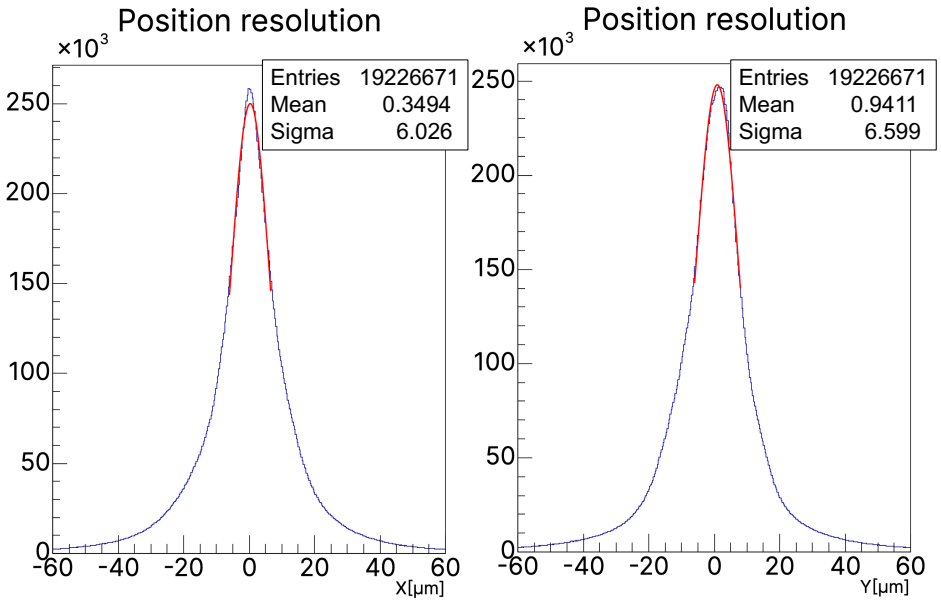

Figure 4.5: Position resolution histograms. The unit of the position is a micrometer.

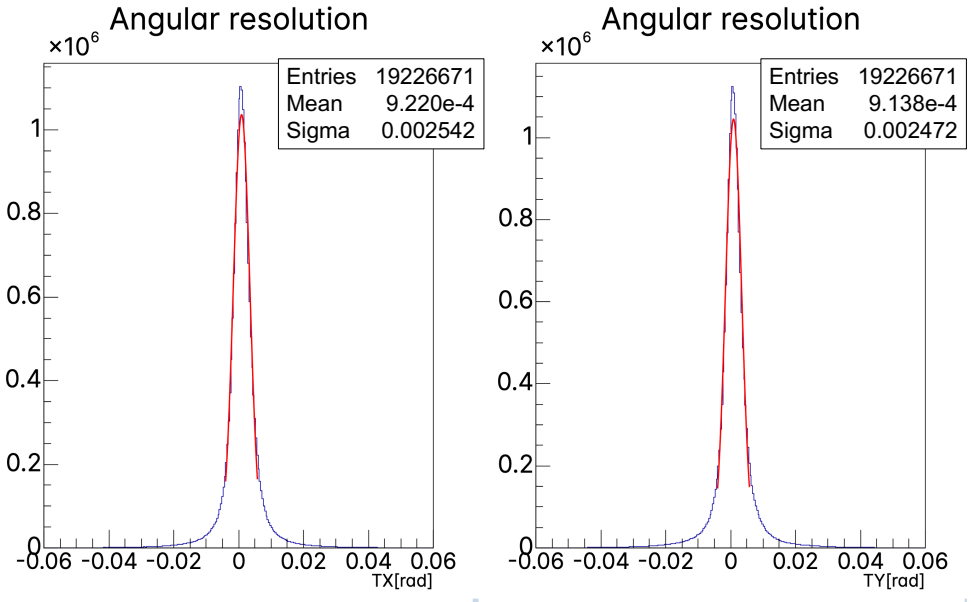

Figure 4.6: Angular resolution histograms. The unit of the angle is radian.

mined axis. Thus, the local alignment creates a local reference frame that makes it possible to relate the locations and orientations of particle tracks to the surface of the film.

The benefit of local alignment is that it guarantees that the data obtained from each emulsion film is calibrated and positioned accurately within their respective coordinate systems. This process is essential for precisely reconstructing the particle paths through the emulsion film. After each film has undergone local alignment, additional procedures can be done to connect and align these films globally, establishing a common reference frame for the whole emulsion stack.

Within the context of this thesis, to compare the local alignment with the global alignment in emulsion films, a square area of $1cm^2$x$1cm^2$ was selected in the center of the consecutive 31 emulsion films, and the position and angular resolution distributions were examined. Position and resolution distributions are illustrated in Figure 4.7 and 4.8. The sigma values of the position resolution distributions (σ_x and σ_y) are about 6 micrometers in global alignment results, while σ_x is about 3 micrometers and σ_y is about 4 micrometers in local alignment results. For angular resolution distributions, σ_{θ_x} and σ_{θ_y} are about $3x10^{-3}$ radian in global alignment results, while they are about $2x10^{-3}$ radian in local alignment results. Comparing the sigma values of the distributions, it can be mentioned that local reconstruction of the data corrects shrinkage differences and improves resolution.

4.3.3 Tracking

With the global alignment achieved, particle tracks traversing multiple emulsion films within the brick can be precisely reconstructed. The track reconstruction procedure for aligned emulsion films requires combining the base-tracks produced in the emulsion films to reconstruct the trajectory of particles inside the target volume. This reconstructed trajectory is also referred to as a "volume-track".

The track reconstruction technique is based on the Kalman Filter algorithm developed in the FEDRA. The Kalman Filter algorithm evaluates the process parameters in a step-by-step way, including information from each new measurement. As additional

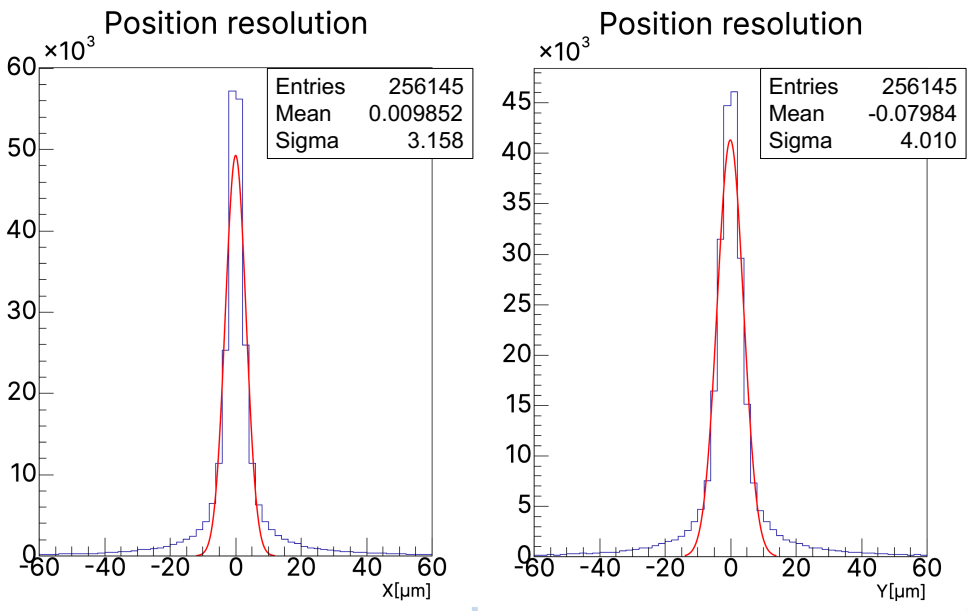

Figure 4.7: Position resolution distributions in the small area.

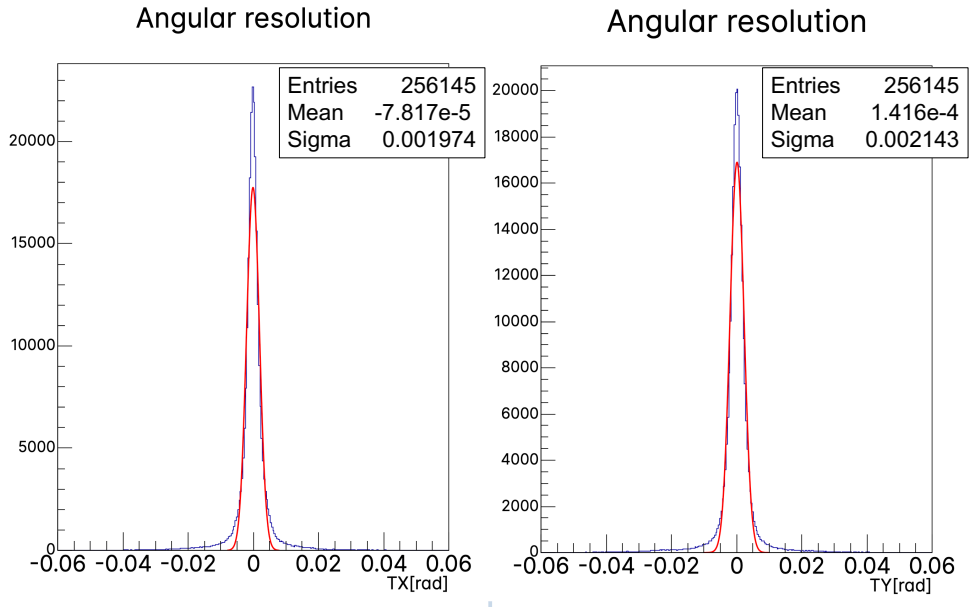

Figure 4.8: Angular resolution distributions in the small area.

measurements are taken into consideration iteratively, the information on the present process parameters continuously improves. The Kalman Filter algorithm takes the initial base-tracks and makes them more accurate and precise through iterative adjustments based on additional information and measurements. Using this information, the algorithm fits the best track estimation at a given z for each measured (real) base-track.

The base-tracks (segments) from consecutive emulsion films are combined once the emulsion films have been aligned and their local coordinate systems have been set up consistently. The base-tracks in different emulsion films are connected during the merging phase to provide a more complete particle trajectory.

In summary, track reconstruction in aligned emulsion films includes combining base-tracks to create volume-tracks, representing the particles' paths inside the target volume. These reconstructed tracks are improved primarily using the Kalman Filter algorithm. The reconstruction procedure aims to identify neutrino interactions and reconstruct their interaction vertices accurately, allowing for a better understanding of particle behavior and interactions within the experimental setup. Detecting neutrino interactions is one of the main objectives of track reconstruction. Connecting the data acquired from the SciFi plane is required for this.

4.3.4 Vertexing

In SND@LHC, vertexing means identifying the interaction points where particles have interacted within the target. This is essential for understanding neutrino interactions. To achieve this, the Emulsion Cloud Chamber of SND@LHC functions as a tracking device that can detect particles interacting in the target and identify various topologies. Vertex detection with micrometric resolution is made possible by the precise segmentation of active emulsion films placed between tungsten plates. By tracking the paths of all created charged particles and reconstructing the interaction vertex, the emulsion reconstruction's primary task is identifying neutrino interactions. The segments of reconstructed tracks are used as starting points for the Kalman Filter used in FEDRA to do this vertex reconstruction.

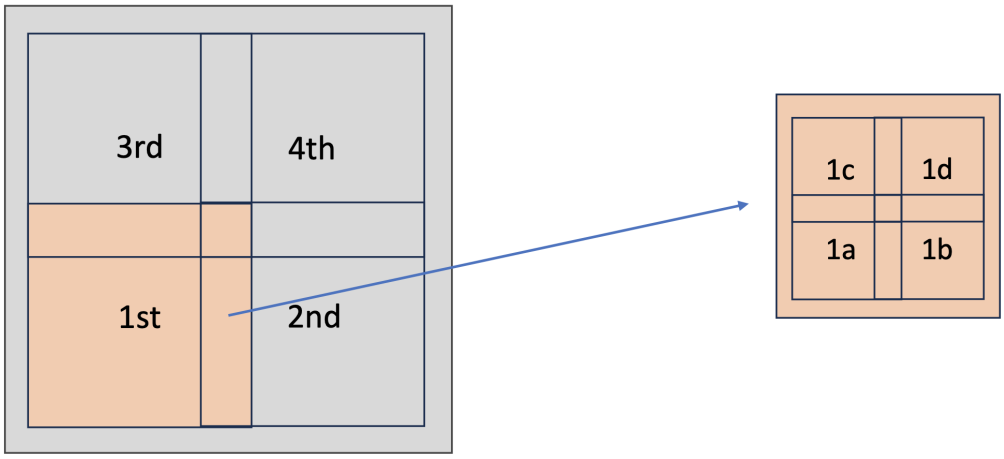

Figure 4.9: Illustration of 4 quadrants (left) and 4 subquadrants of the 1^{st} quarter (right).

In this thesis work, Emulsion RUN0 data consisting of 31 consecutive emulsion films is studied. The scanned emulsion surface is 180 x 180 mm^2. Tracking has been performed separately in four different regions of size 96 x 96 mm^2 considering 5% surface overlap, named "quadrant". Tracks within the overlapping region are considered once. For the vertex reconstruction, quadrants are divided into four regions of size 53 x 53 mm^2 considering 10% overlap, named "subquadrant". Vertices within the overlap region are taken into account once. There are 4 quadrants for tracking and 16 subquadrants for vertexing in total. Figure 4.9 demonstrates an illustration of this representative division.

4.4 Emulsion RUN0 Analysis

The number of vertices reconstructed in the sample is about $3x10^6$. The expected neutrino interaction for RUN0 is smaller than one; the primary purpose of this study is to improve the vertexing quality.

For the vertices to be in analyzed volume, the z position of the starting and the end point of the volume were given as a cut for the z position of the vertices. Then, the χ^2 of linear track fit of the tracks in the vertices within the analyzed volume is estimated after obtaining the position and angular resolution distributions shown in Figure 4.6 and 4.7. A sigma value is determined for both position and angular resolution distributions. For the position resolution distributions, the value for both σ_x and σ_y is about 6 micrometers and for the angular distributions, both σ_{θ_x} and σ_{θ_y} are about $3x10^{-3}$ radian. The χ^2 of each linear track fit is calculated according to these sigma values and with position and angular residuals; Δx, Δy, $\Delta\theta_x$, $\Delta\theta_y$, as in

$$\chi^2 = \frac{\Delta x^2}{\sigma_x^2} + \frac{\Delta y^2}{\sigma_y^2} + \frac{\Delta\theta_x^2}{\sigma_{\theta_x}^2} + \frac{\Delta\theta_y^2}{\sigma_{\theta_y}^2} \tag{4.1}$$

where Δx and Δy are the difference (residual) between the position of each segment of each track and the position of the linear fit, and $\Delta\theta_x$ and $\Delta\theta_y$ are the difference between the angles of the segments and the linear track fit slope. After the iteration of this calculation over all vertices, the χ^2/ndof distribution is obtained, as illustrated in Figure 4.10. Also, the number of segments of each track is identified, and the χ^2/ndof versus the number of segments (nseg) plot is obtained, as illustrated in Figure 4.11.

To eliminate the fake vertices, in accordance with the χ^2/ndof distribution, the tracks with the χ^2/ndof $\geq$ 20 are not used for the vertexing. Figure 4.11 shows χ^2/ndof as a function of track segments. After nseg>4, χ^2/ndof reaches a plateau. Therefore, tracks with nseg>4 are used in vertexing. In addition to those selections, vertices with more than 3 tracks are considered to suppress the fake reconstruction.

Then, the impact parameters (Ip) were checked for vertexing quality and compared results to determine if the selection criteria applied on the tracks and vertices made it better. In Figure 4.12, the black line represents the impact parameter distribution of the tracks in the vertices within the analyzed volume with the cut on only the number of tracks (ntracks) that is larger than 2, and the red line represents the impact parameter distribution of the tracks in the vertices with the number of tracks larger than 3, χ^2/ndof is smaller than 20, and the number of segments of tracks is larger than 4.

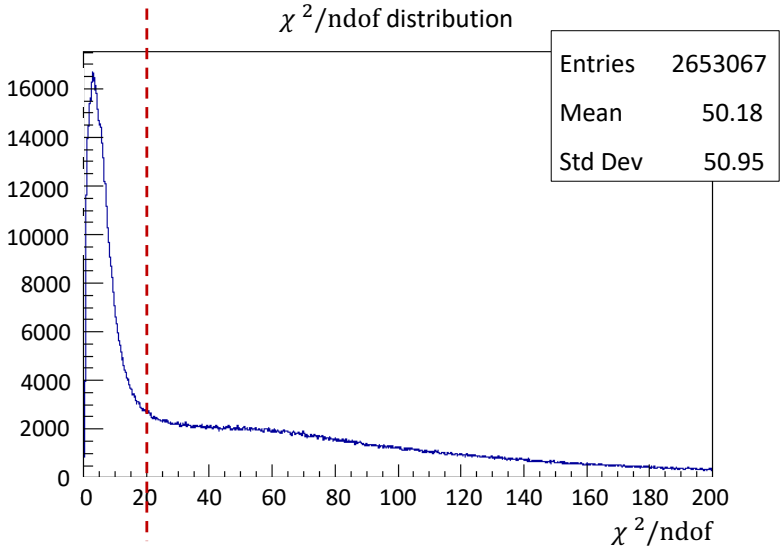

Figure 4.10: The χ^2/ndof distribution.

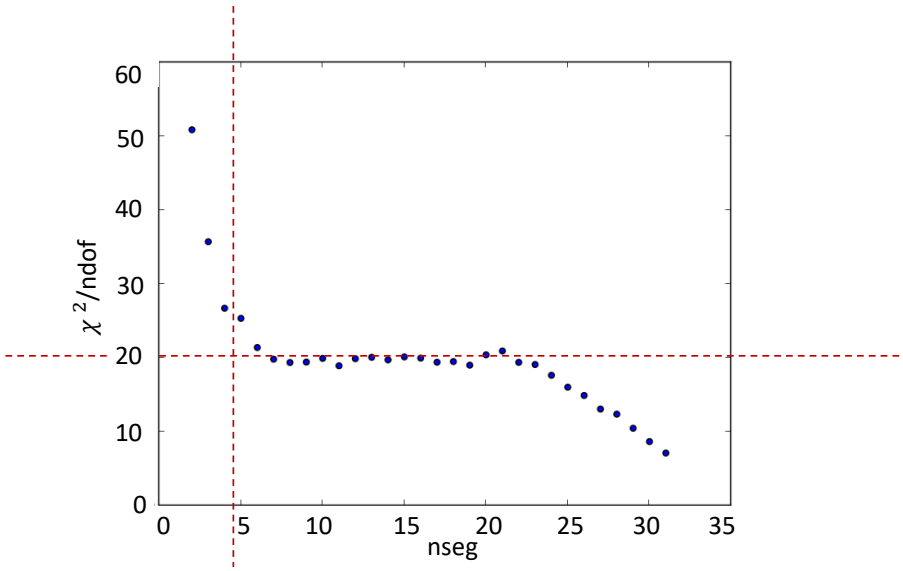

Figure 4.11: The graph of χ^2/ndof versus number of segments.

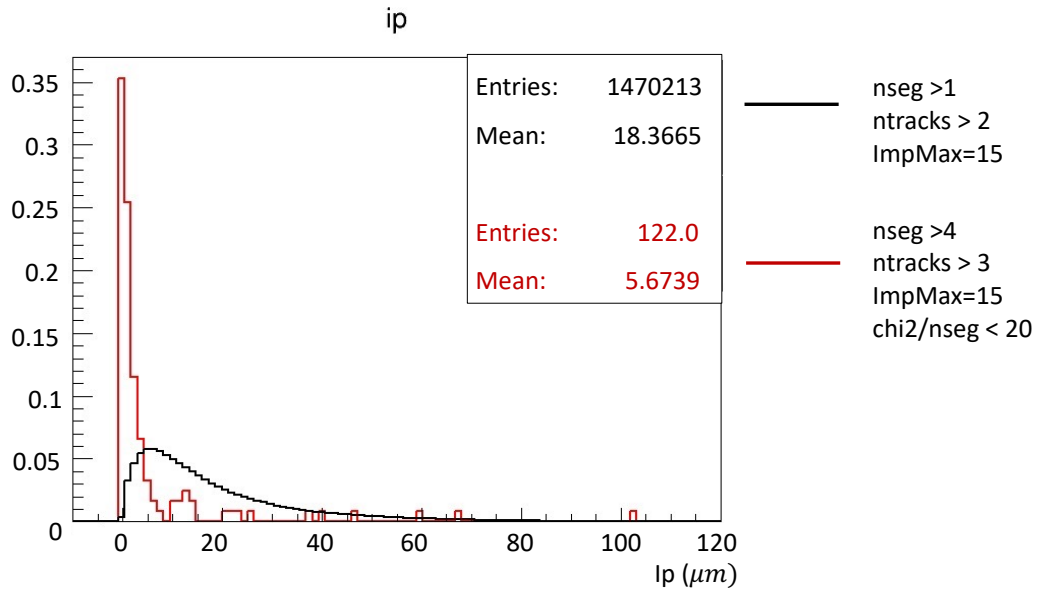

Figure 4.12: Impact parameter distribution. Black (default) and red lines represent the selection criteria applied. The unit of Ip is a micrometer.

In Figures 4.12 - 4.16, the black lines represent the default FEDRA selection criteria, whereas the red lines represent the selection criteria applied for the studies of this thesis.

Applying selection criteria on tracks and vertices, a significant improvement in impact parameter values is observed; the mean value of the impact parameter distribution decreased from about 18 to about 5.

Since the impact parameter is important for vertexing quality, the maximum impact parameter for two-track vertices is set to 10 micrometers (ImpMax=10) for comparison. After this cut, the multiplicity distribution of vertices is checked and compared, as shown in Figure 4.13. When the mean values are compared, it is seen that the mean value of the multiplicity increased from about 3 to about 5, as expected.

After applying these four selection criteria, vertex topologies are analyzed through a *flag*, which provides information about the vertex topology as illustrated in Figure 4.14. Vertices with flag 0(3) mean neutral forward (linked) vertices, flag 1(4) mean charged forward (linked) vertices, and flag 2(5) mean neutral backward (linked) vertices [10]. The flags in the parenthesis, flag 3, flag 4, and flag 5, indicate that they

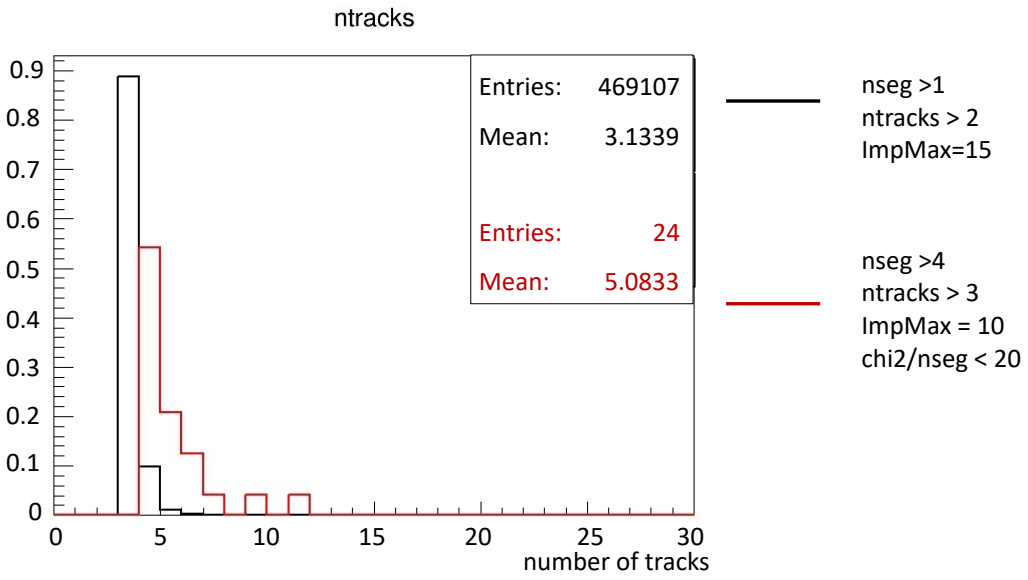

Figure 4.13: Multiplicity distribution of vertices. Black (default) and red lines represent the selection criteria applied.

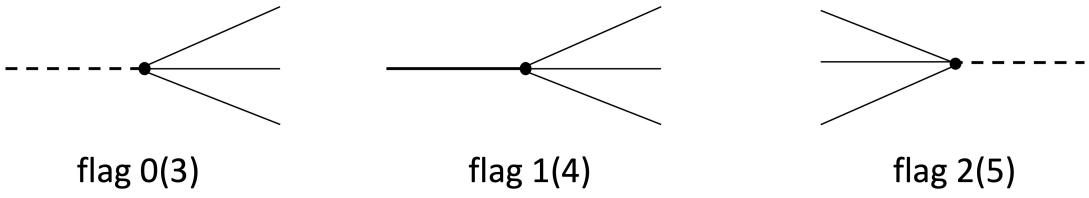

Figure 4.14: Vertex topologies indicated by flag 0(3), flag 1(4) and flag 2(5).

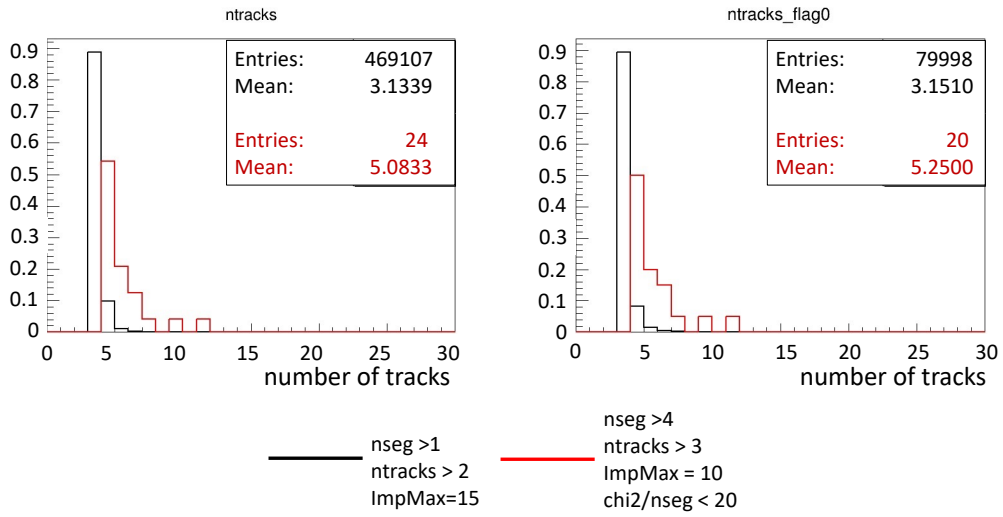

Figure 4.15: Multiplicity distribution of vertices for all flags (left) and for flag 0 and flag 3 (right). Black (default) and red lines represent the selection criteria applied.

are linked vertices, meaning they are the vertex with at least one track in common with another vertex. Then, the vertex flag needed to be 0 or 3 for the neutrino event. Applying the criteria flag is 0 or 3 with the aim of a neutrino event; multiplicity distributions were compared as illustrated in Figure 4.15. After all selection criteria are applied, the number of vertices remaining is 20. Then, the fake vertices are eliminated with these selection criteria.

If the impact parameter distributions of the tracks in the vertices with flag 0(3) are compared, a significant improvement is seen in the impact parameter values with the applied selection criteria. The mean value of the impact parameter distribution for the flag 0(3) events decreased from about 20 micrometers to 1.85 micrometers, as shown in Figure 4.16.

In summary, there are $3x10^6$ vertices in the sample. For vertices to be inside the analyzed volume, a z-position cut is applied as default. In this study, to improve the vertexing quality in this volume, different selection criteria are applied. Table 4.1 represents a comparison of the number of vertices, the mean value of the impact parameters (Ip) of the tracks, and the mean value of the multiplicity between the default FEDRA reconstruction and the reconstruction with selection criteria applied.

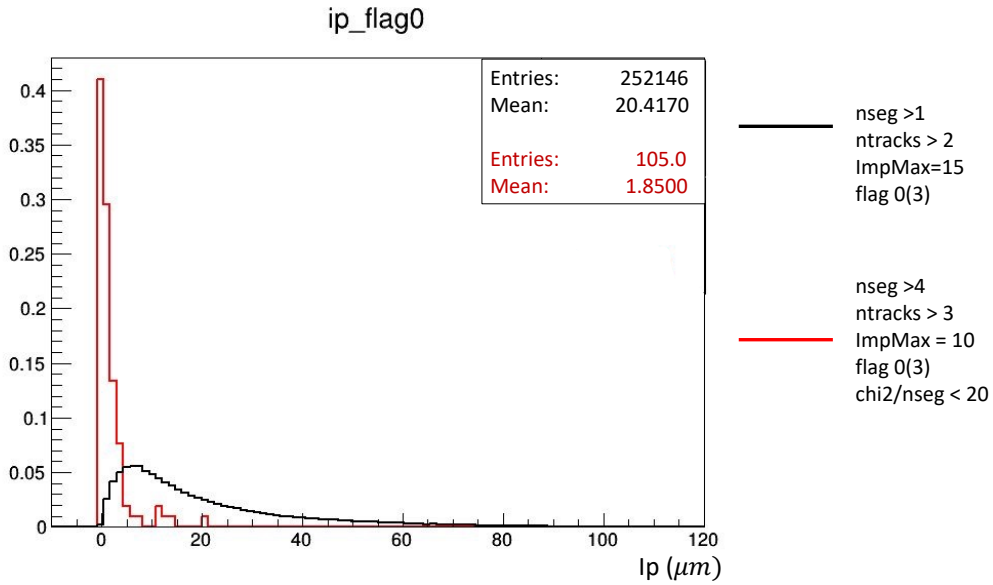

Figure 4.16: Impact parameter comparison for flag 0(3) events. Applied selection criteria are represented with black (default) and red lines.

Table 4.1: Comparison of the vertices in the analyzed volume (z cut is applied for all vertices).

	nseg>1 ntracks>2 ImpMax=15	nseg>1 ntracks>2 ImpMax=15 flag 0(3)	nseg>4 ntracks>3 ImpMax=10 flag 0(3) chi2/nseg<20
number of vertices	469107	79998	20
mean value of the Ip (μm)	18.4	20.4	1.9
mean value of the multiplicity	3.1	3.2	5.3

4.4.1 3D Display of Reconstructed Tracks

Event Display and Analyser (EDA) is a class in the FEDRA that can be used to display a three-dimensional view of the reconstructed particle tracks traversing the emulsion films [1]. This display shows the trajectories taken by particles as they pass through the emulsion films. All 20 vertices passing the selection criteria are visualized in Appendix A.

CHAPTER 5

CONCLUSION

The SND@LHC experiment aims to observe energetic neutrinos in all flavours produced at the LHC. In addition, it is also capable of detecting feebly interacting particles (FIPs). The SND@LHC detector was installed during the Long Shutdown period in TI18, 480 m downstream of the ATLAS interaction point along the beam collision axis. It is an off-axis experiment and covers the unexplored pseudo-rapidity range of $7.2 < \eta < 8.4$. It will collect 250 fb^{-1} of data during Run 3 of the LHC. The data taking was started in 2022, and the first period is called "Emulsion RUN0", whose data is used to test emulsion data reconstruction steps, including emulsion scanning and subsequent reconstruction steps. In this thesis work, the Emulsion RUN0 Data is analyzed for possible improvements in tracking and vertexing. A new track selection criteria based on the χ^2 is developed and implemented in the tracking algorithm. A significant reduction in the number of false tracks and vertices was obtained while improving the vertex quality in terms of impact parameter and multiplicity distributions. The track multiplicity of the reconstructed vertices is increased from about 3 to about 5. Also, the mean value of the impact parameter distribution of the tracks is decreased from about 18 to 1.85 micrometers, which implies a notable improvement in the vertexing quality.

Since the number of expected neutrino interactions for RUN0 is smaller than one, it is not expected to observe a neutrino event. The result of this study on vertexing quality may help search for neutrino interactions in the following emulsion runs. 3-D event display of the 20 vertices visualized in the end. Some of these events can be neutral particle interactions or decay. It requires additional analysis to identify the nature of these selected events.

REFERENCES

[1] Fedra emulsion software from the opera collaboration. `https://www.neutrino-exp.unina.it/fedradoxygen/index.html` [Accessed: (August 19, 2023)].

[2] C. Ahdida, M. De Magistris, M. Gorshenkov, E. Zaffaroni, L. Dedenko, M. Chernyavskiy, V. Tioukov, J. Grenard, G. Vankova-Kirilova, S. Shirobokov, et al. Snd@lhc-scattering and neutrino detector at the lhc. Technical report, 2021.

[3] R. Albanese, A. Alexandrov, F. Alicante, A. Anokhina, T. Asada, C. Battilana, A. Bay, C. Betancourt, R. Biswas, A. B. Castro, et al. Observation of collider muon neutrinos with the snd@lhc experiment. *Physical Review Letters*, 131(3):031802, 2023.

[4] R. G. Alía, M. Brugger, F. Cerutti, S. Danzeca, A. Ferrari, S. Gilardoni, Y. Kadi, M. Kastriotou, A. Lechner, C. Martinella, et al. Lhc and hl-lhc: Present and future radiation environment in the high-luminosity collision points and rha implications. *IEEE Transactions on Nuclear Science*, 65(1):448–456, 2017.

[5] A. Blondel, P. Böckmann, H. Burkhardt, F. Dydak, A. Grant, R. Hagelberg, E. Hughes, W. Krasny, A. Para, H. Taureg, et al. Electroweak parameters from a high statistics neutrino nucleon scattering experiment. *Zeitschrift für Physik C Particles and Fields*, 45:361–379, 1990.

[6] C. Collaboration, J. Allaby, U. Amaldi, G. Barbiellini, M. Baubillier, F. Bergsma, A. Capone, W. Flegel, F. Grancagnolo, L. Lanceri, et al. A precise determination of the electroweak mixing angle from semileptonic neutrino scattering. *Zeitschrift für Physik C Particles and Fields*, 36:611–628, 1987.

[7] P. Coloma, B. A. Dobrescu, C. Frugiuele, and R. Harnik. Dark matter beams at lbnf. *Journal of High Energy Physics*, 2016(4):1–20, 2016.

[8] J. M. Conrad, M. H. Shaevitz, and T. Bolton. Precision measurements with high-energy neutrino beams. *Reviews of Modern Physics*, 70(4):1341, 1998.

[9] A. Di Crescenzo and G. Galati. Snd@lhc: A new experiment in neutrino physics at the lhc. *Symmetry*, 15(6), 2023.

[10] A. Iuliano. Basic fedra workflow, 2022. `https://twiki.cern.ch/twiki/bin/view/SndLHC/FedraWorkflow` [Accessed: (August 13, 2023)].

[11] M. Kelsey, R. Cruz-Torres, X. Dong, Y. Ji, S. Radhakrishnan, and E. Sichtermann. Constraints on gluon distribution functions in the nucleon and nucleus from open charm hadron production at the electron-ion collider. *Physical Review D*, 104(5), sep 2021.

[12] SND@LHC Collaboration. Snd@lhc: The scattering and neutrino detector at the lhc, 2023.

[13] G. Sterman, J. Smith, J. C. Collins, J. Whitmore, R. Brock, J. Huston, J. Pumplin, W.-K. Tung, H. Weerts, C.-P. Yuan, et al. Handbook of perturbative qcd. *Reviews of Modern Physics*, 67(1):157, 1995.

[14] F. Suekane. *Weinberg Angle*, pages 57–71. Springer International Publishing, Cham, 2021.

APPENDIX A

EVENT DISPLAY

Event displays of the vertices passing the selection criteria are listed in the following figures. One cannot distinguish between neutral interactions based only on the event displays. Monte Carlo (MC) simulation samples of neutral hadron interaction and neutrino interaction are currently being studied to find the specific characterization of these different neutral vertices. By comparing the event display with the MC simulation results, neutral hadron and neutrino interactions can be distinguished. However, since the expected number of neutrino interactions is smaller than 1 for RUN0 data, this study can be done to study neutral background events.

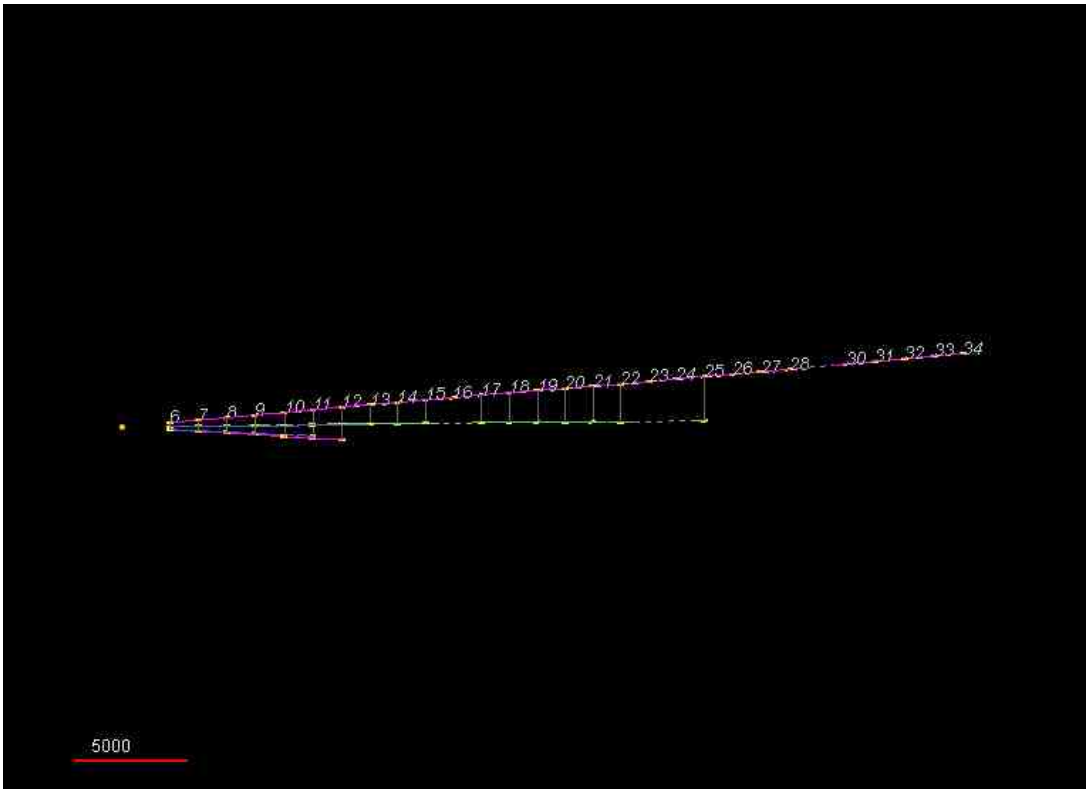

Figure A.1: A vertex with 5 tracks.

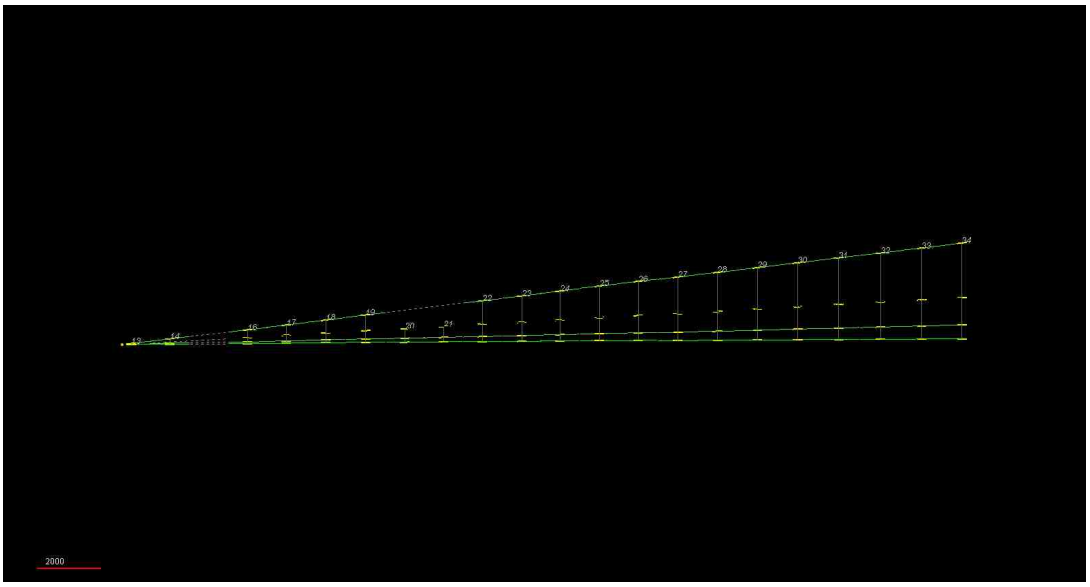

Figure A.2: A vertex with 4 tracks.

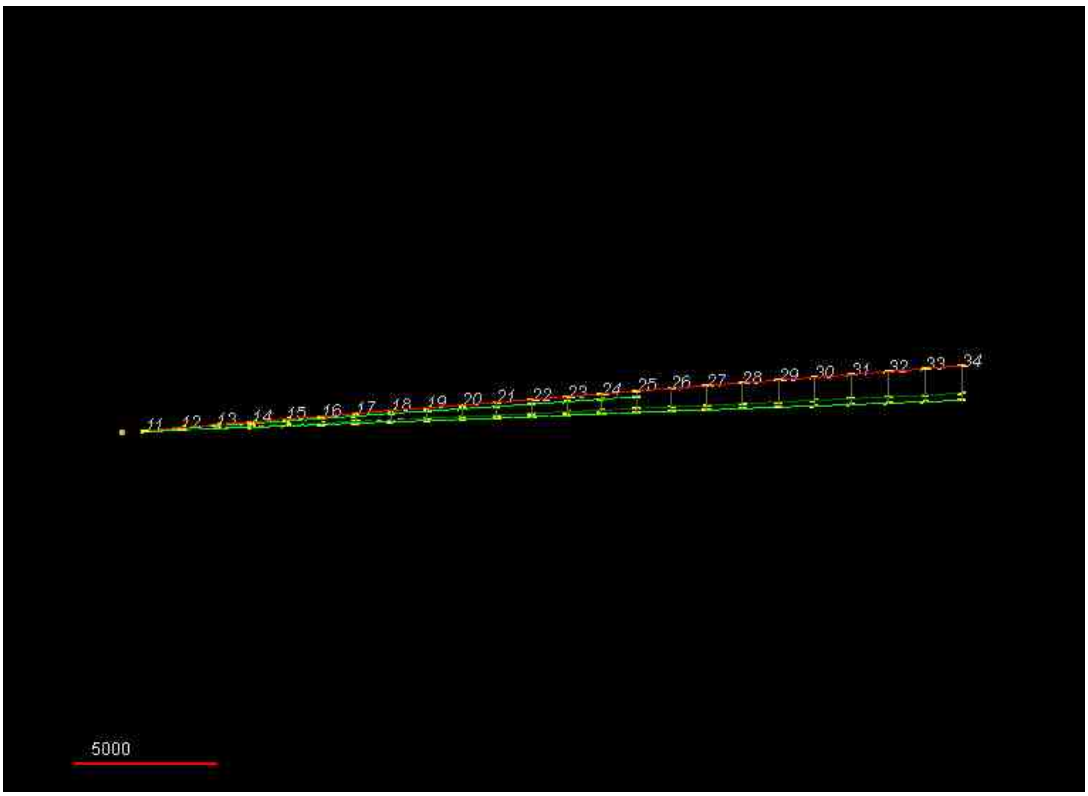

Figure A.3: A vertex with 4 tracks.

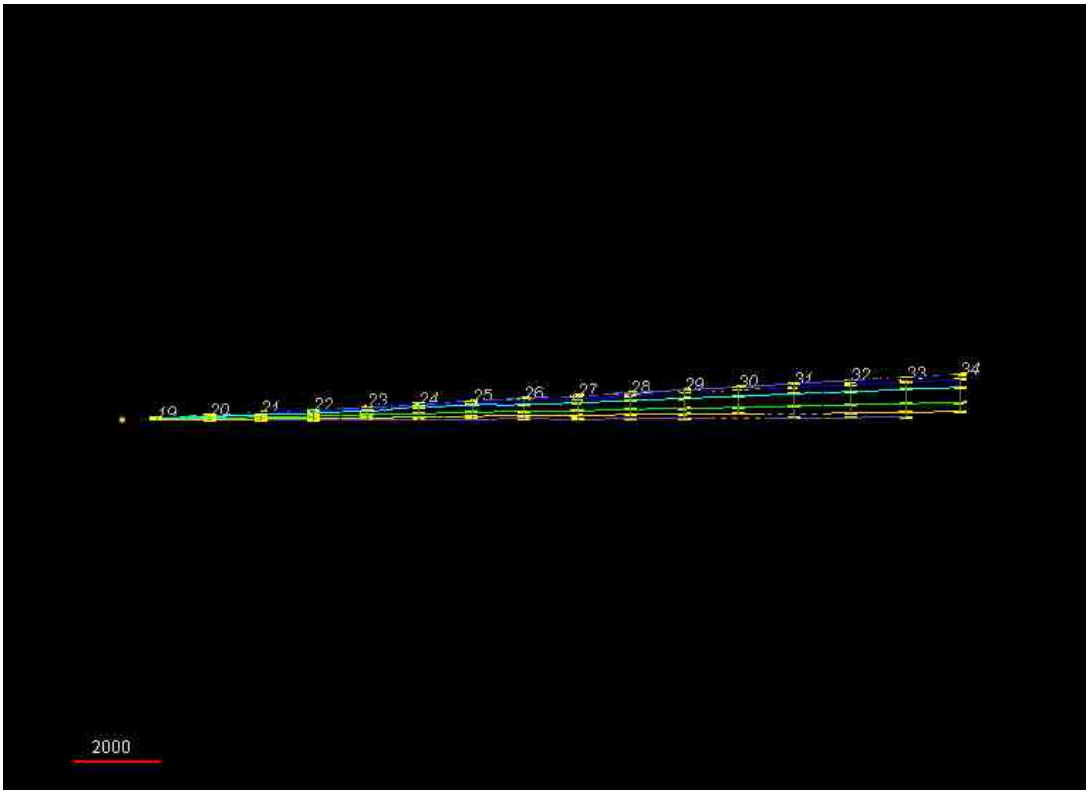

Figure A.4: A vertex with 7 tracks.

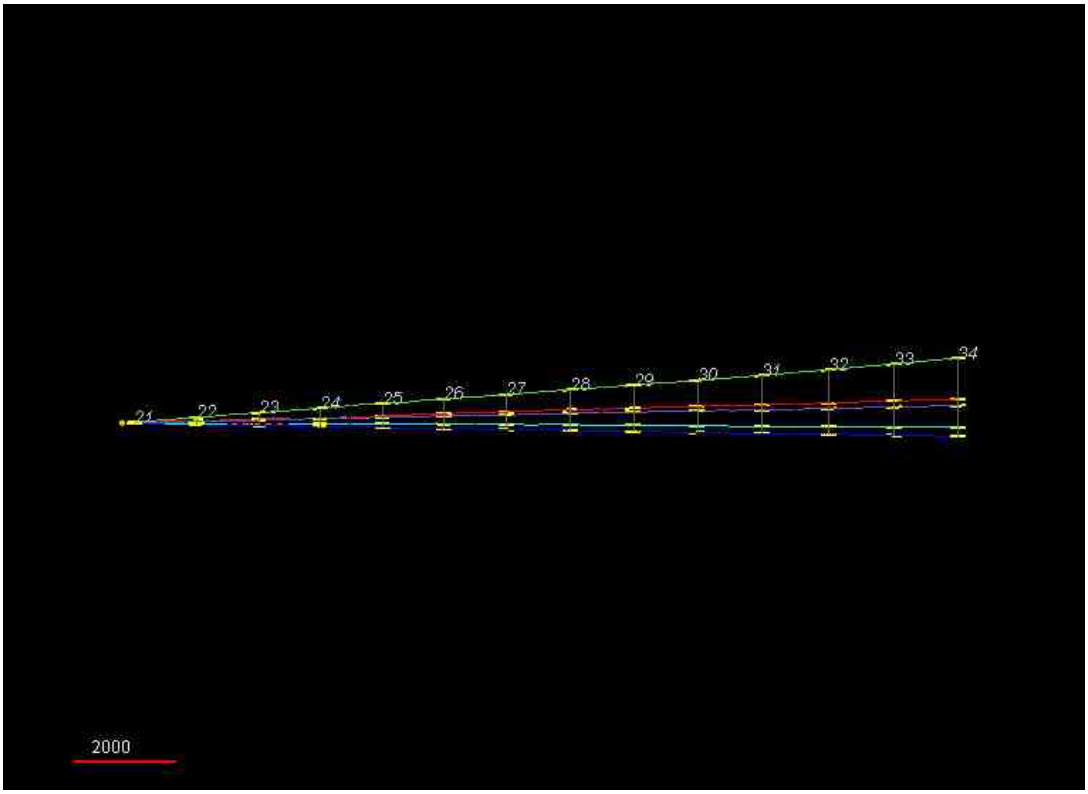

Figure A.5: A vertex with 5 tracks.

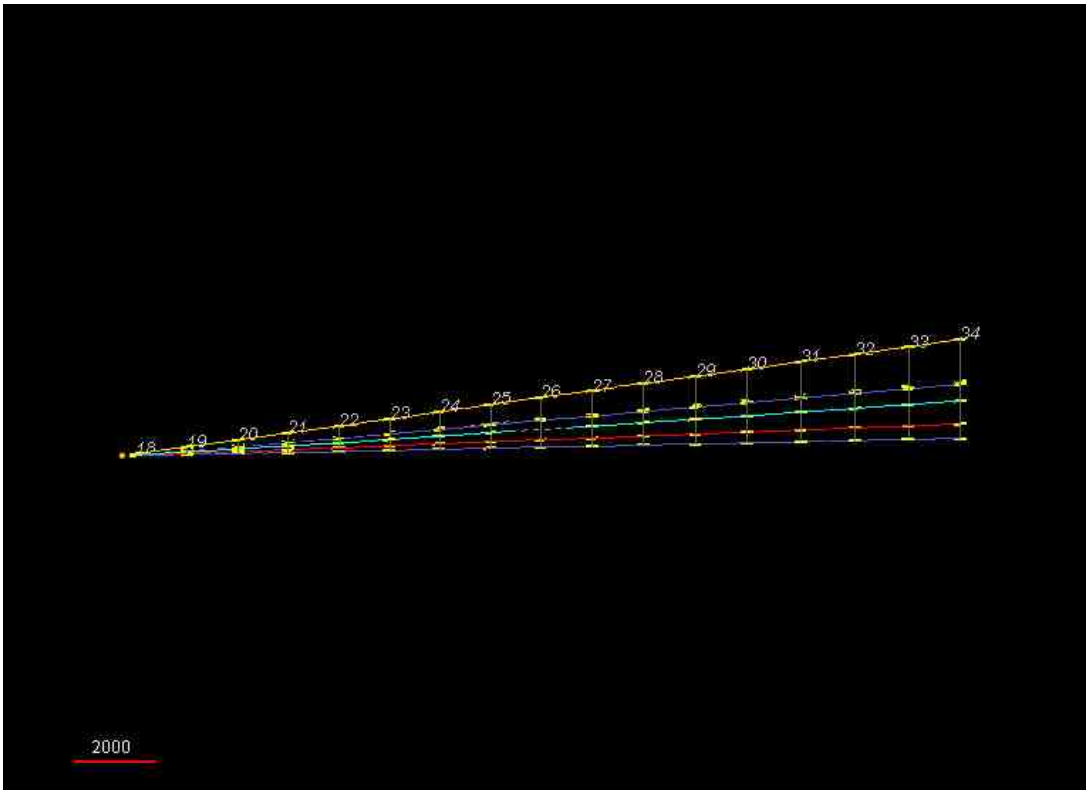

Figure A.6: A vertex with 6 tracks.

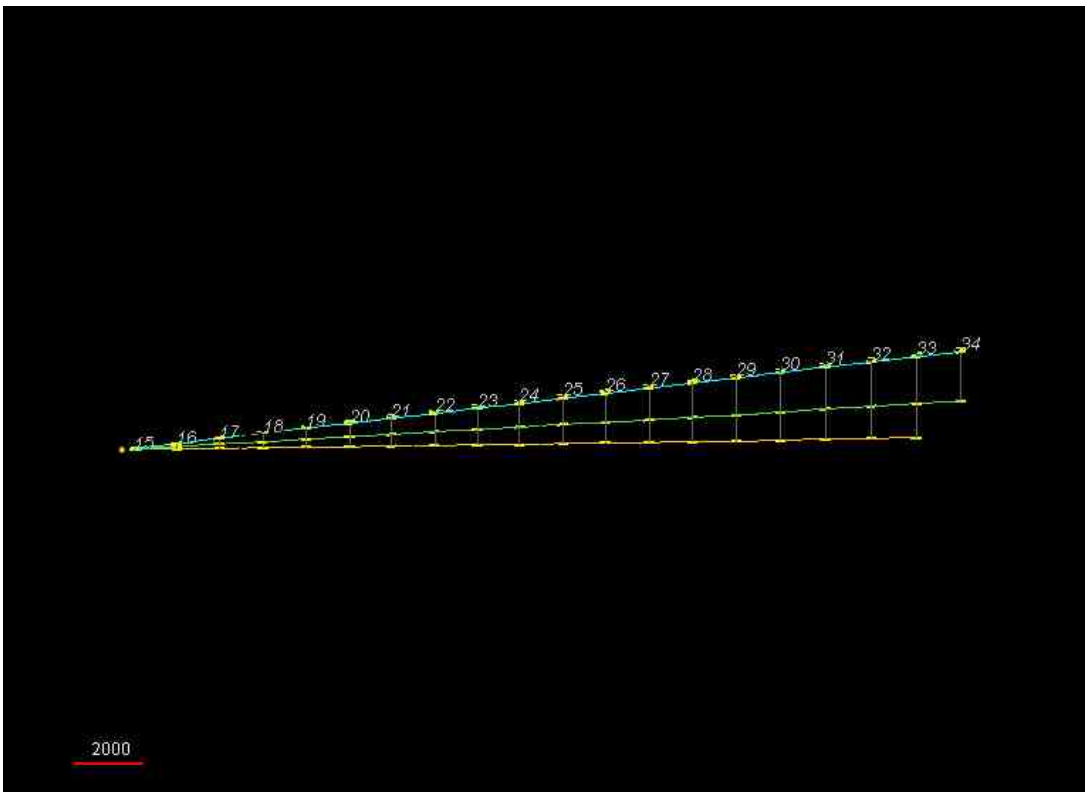

Figure A.7: A vertex with 4 tracks.

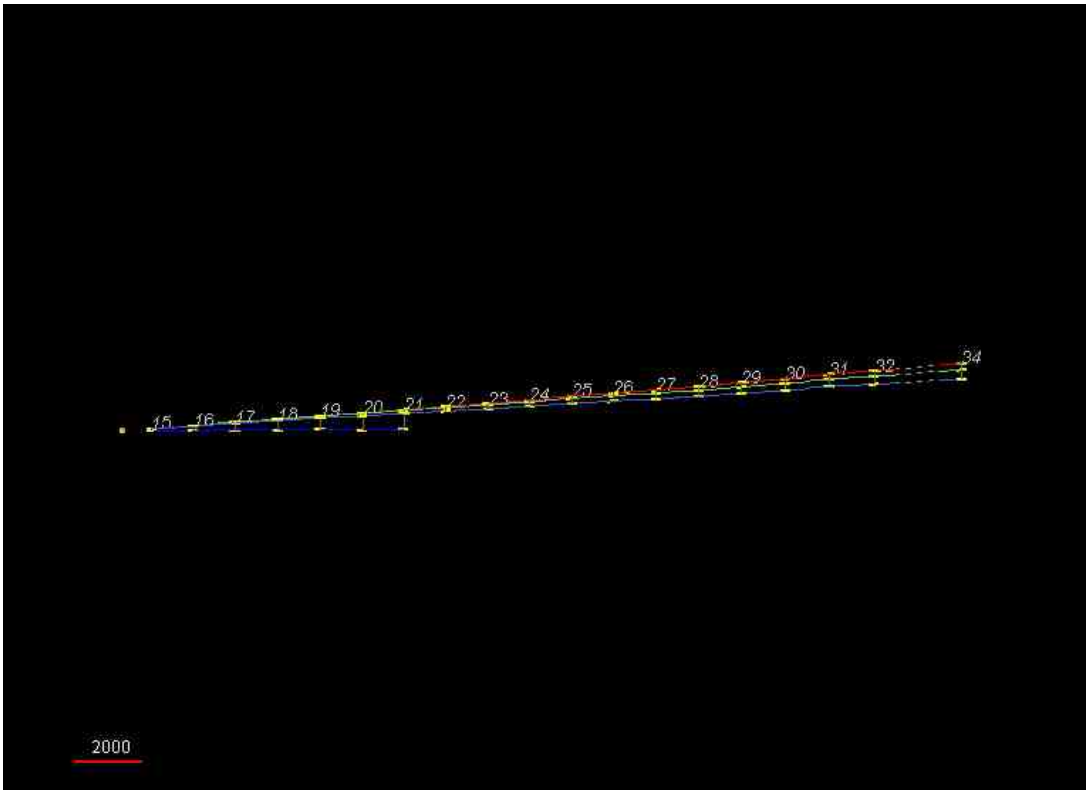

Figure A.8: A vertex with 4 tracks.

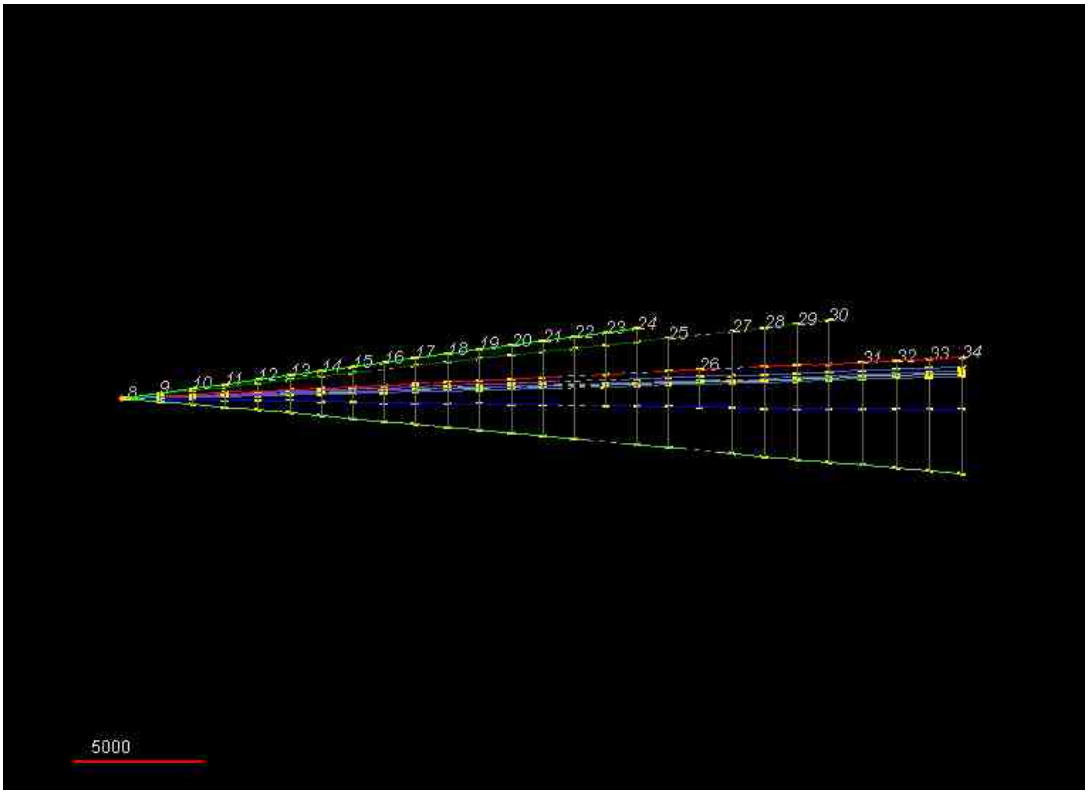

Figure A.9: A vertex with 9 tracks.

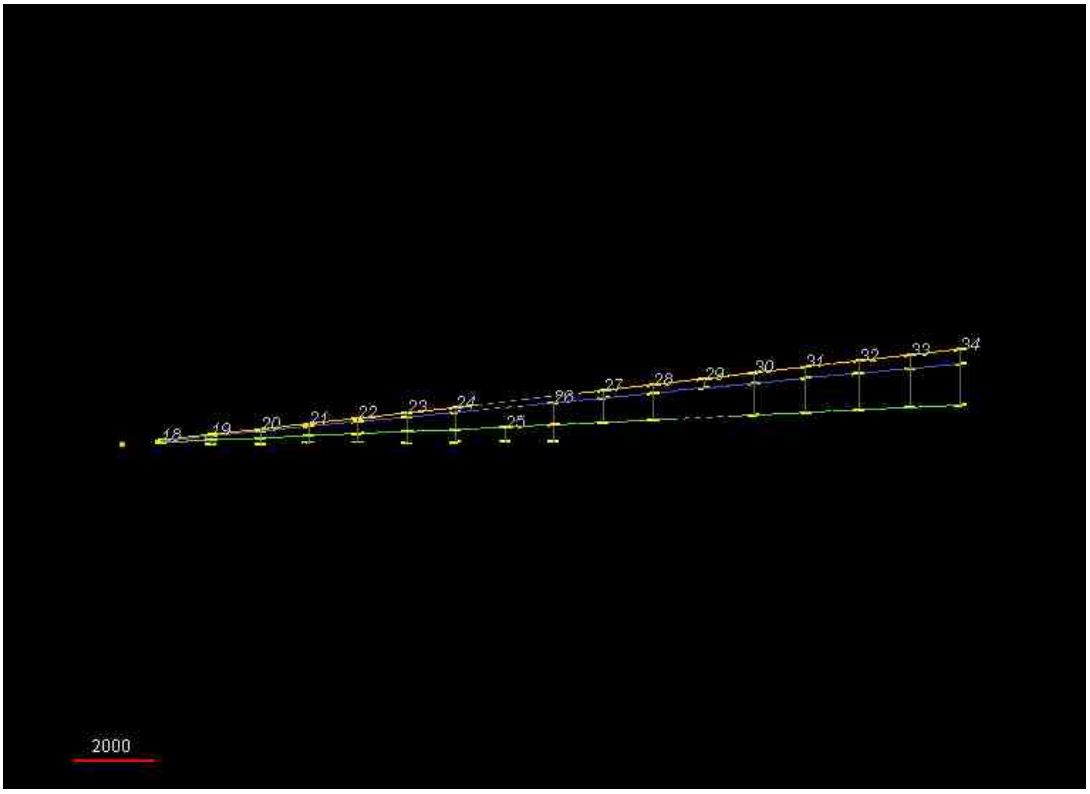

Figure A.10: A vertex with 4 tracks.

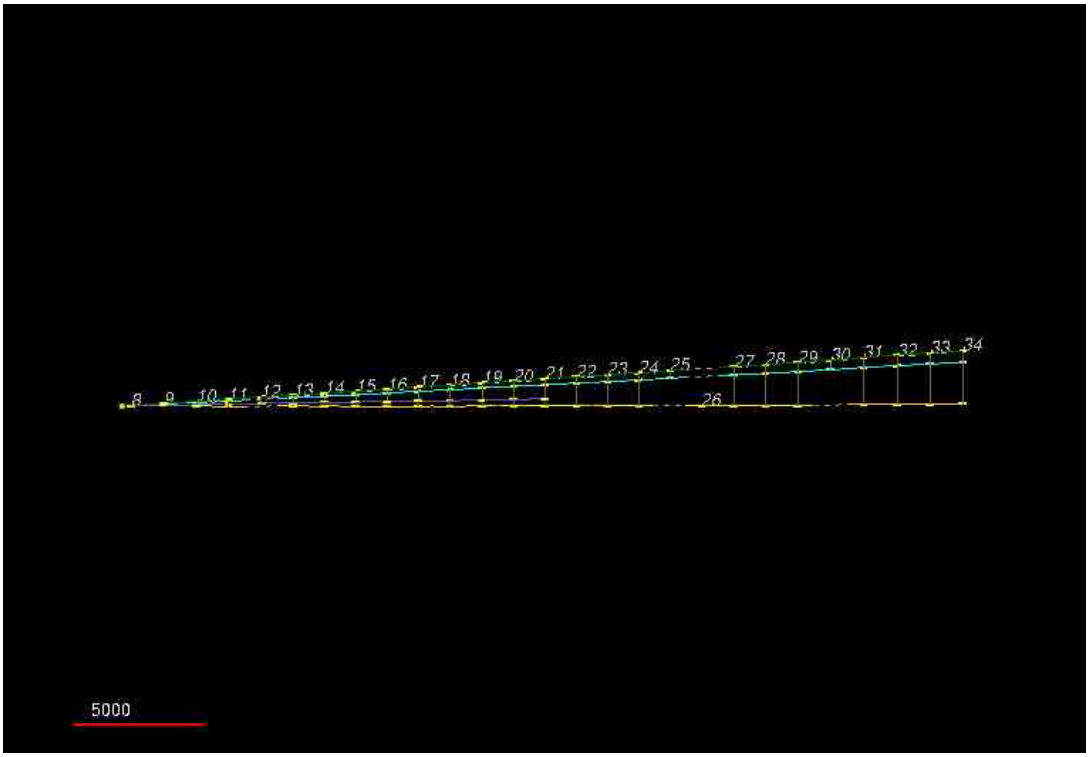

Figure A.11: A vertex with 4 tracks.

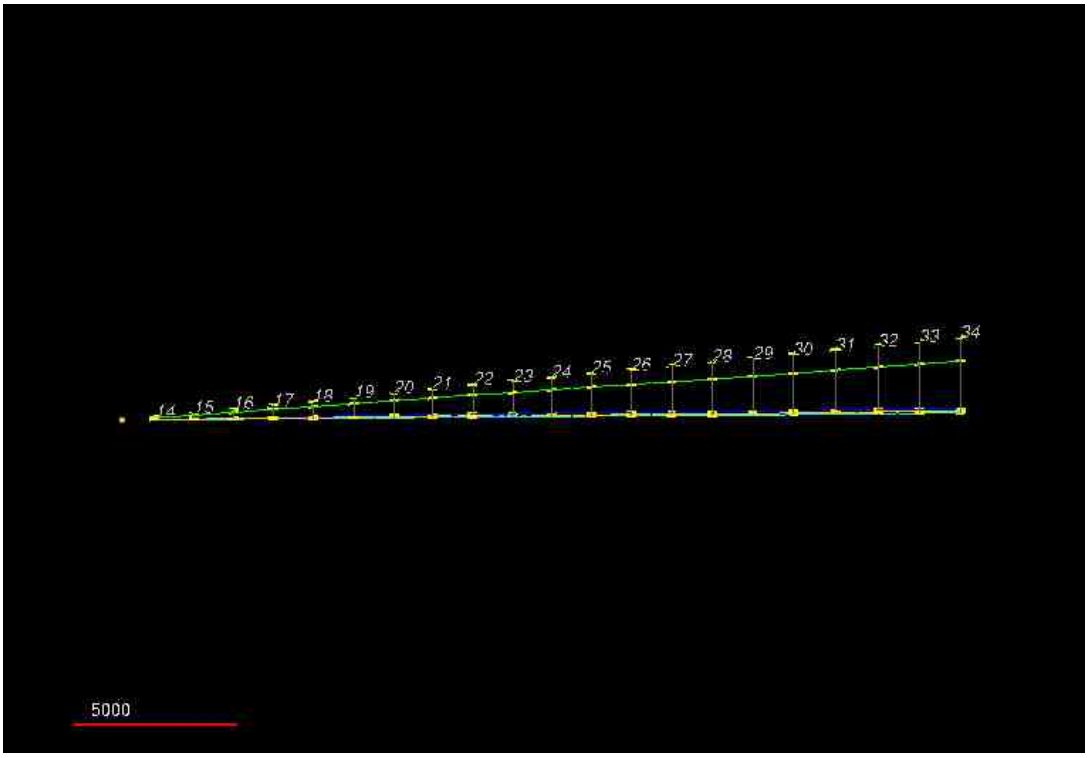

Figure A.12: A vertex with 5 tracks.

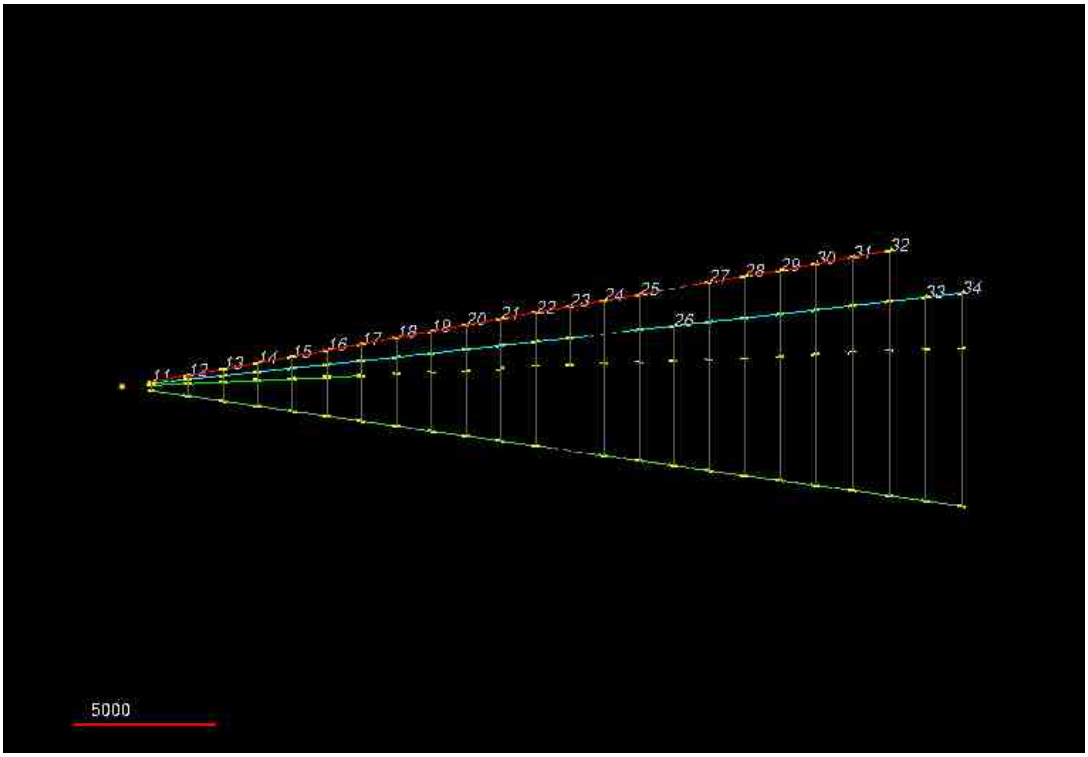

Figure A.13: A vertex with 5 tracks.

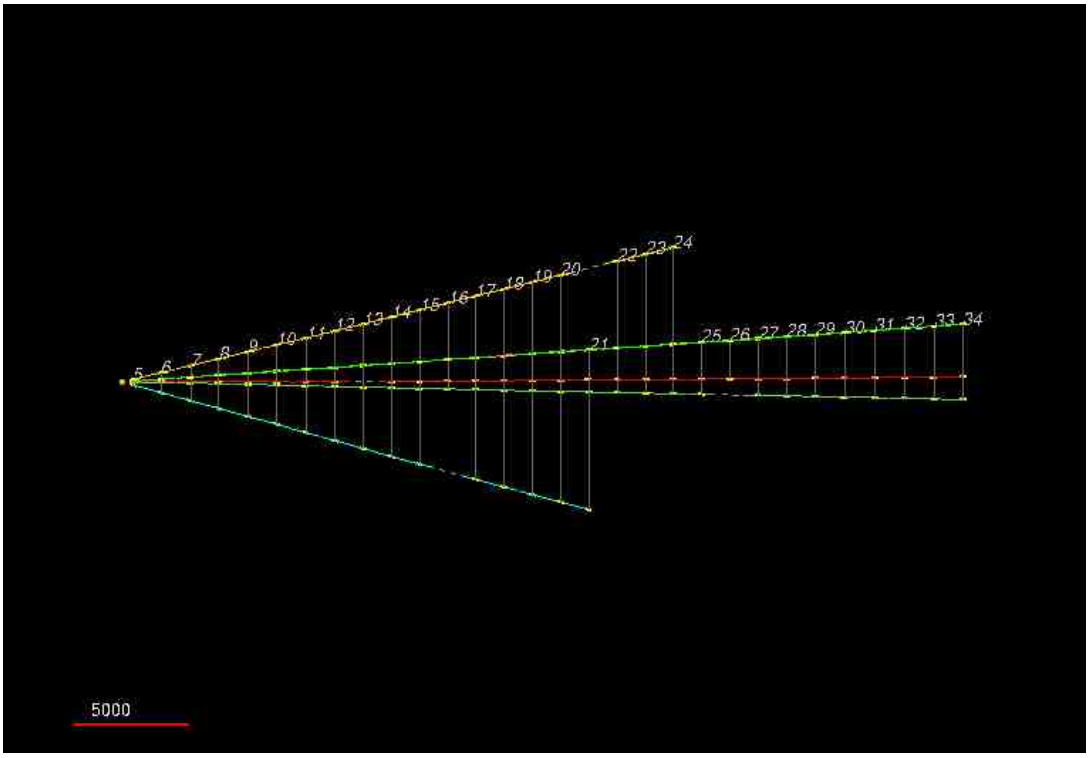

Figure A.14: A vertex with 6 tracks.

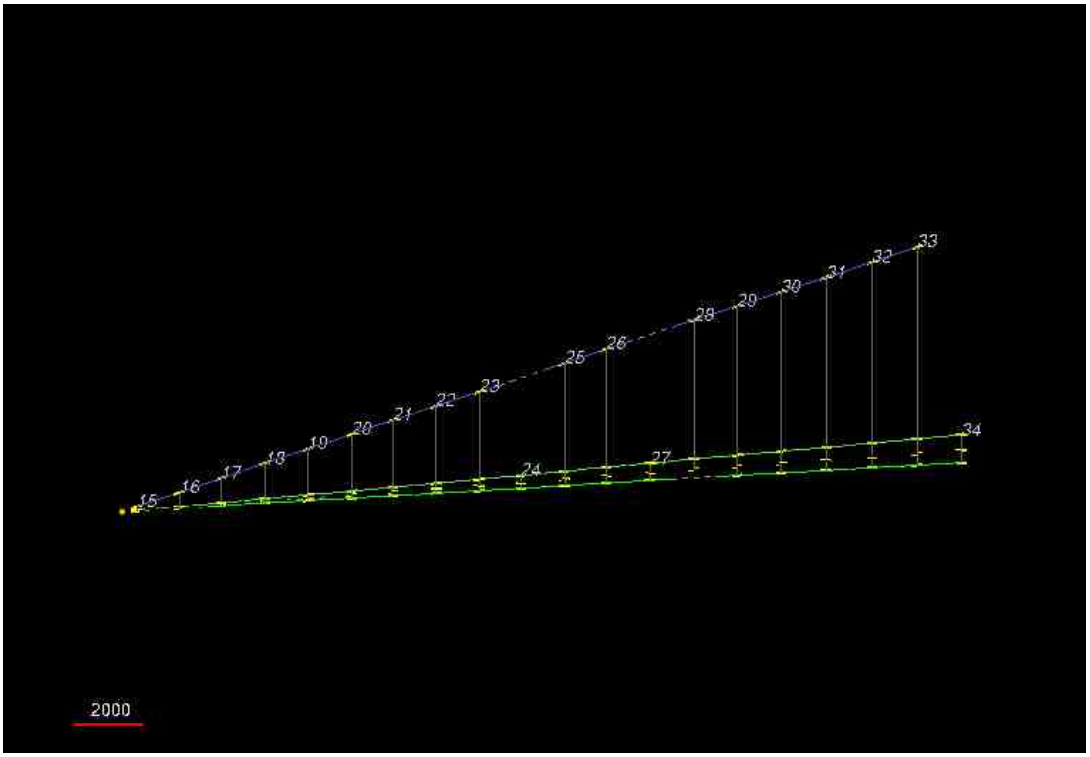

Figure A.15: A vertex with 4 tracks.

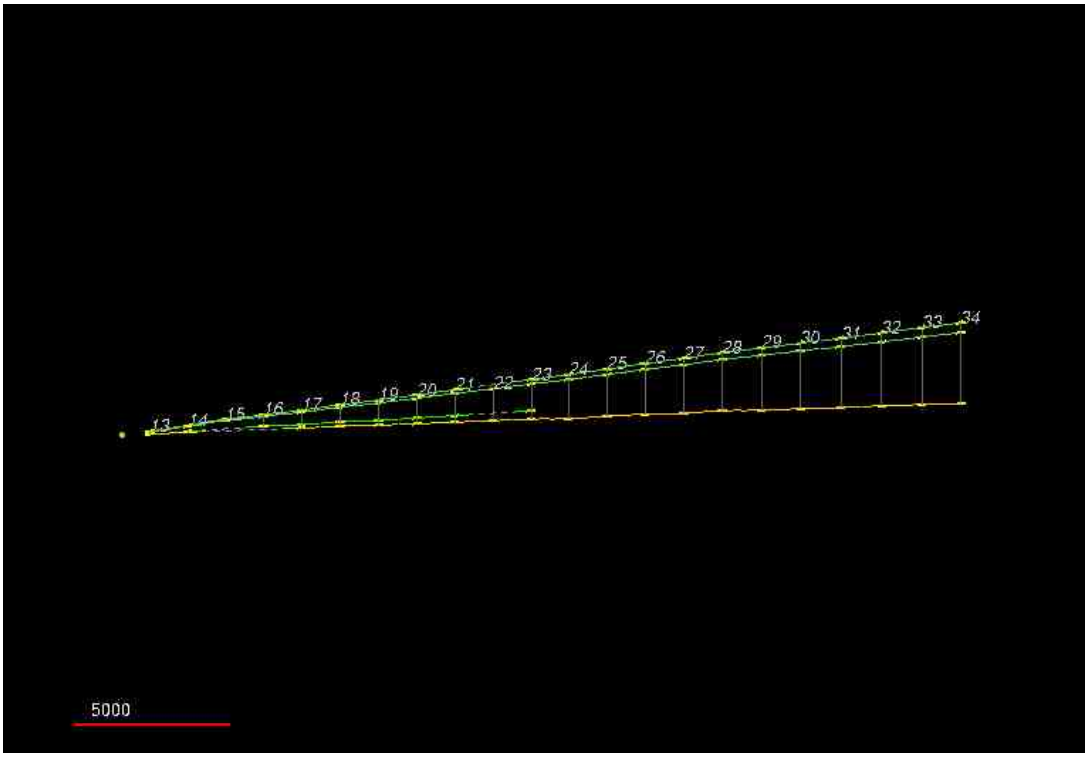

Figure A.16: A vertex with 4 tracks.

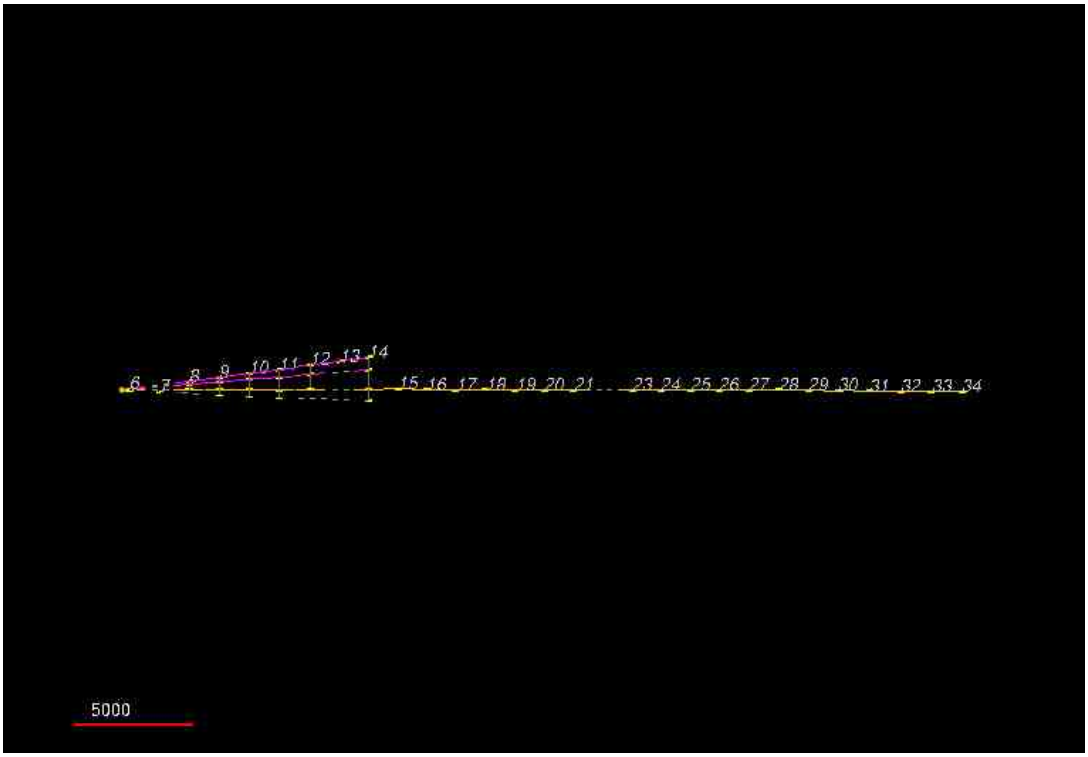

Figure A.17: A vertex with 4 tracks.

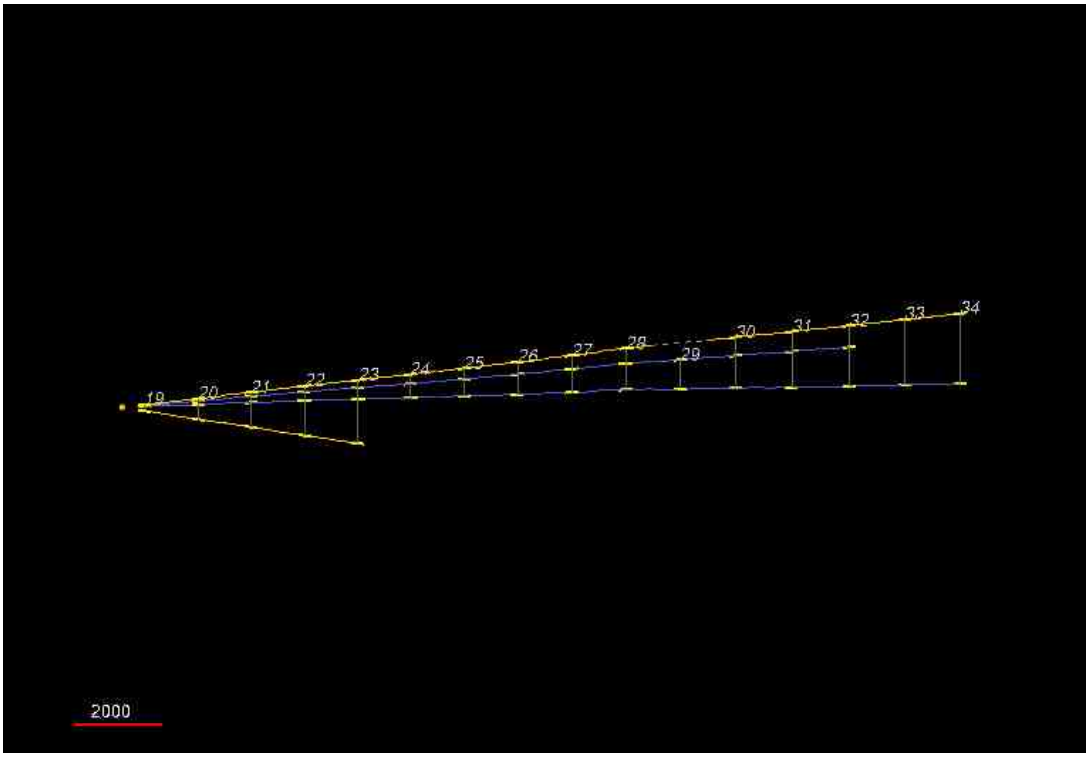

Figure A.18: A vertex with 4 tracks.

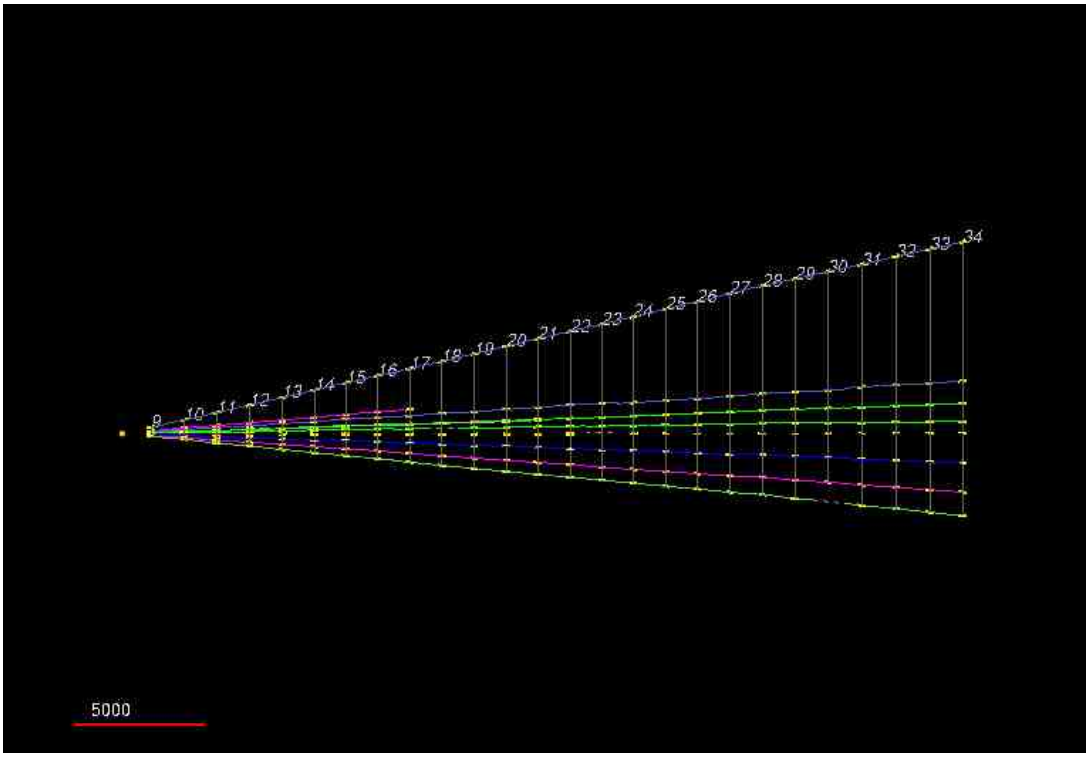

Figure A.19: A vertex with 11 tracks.

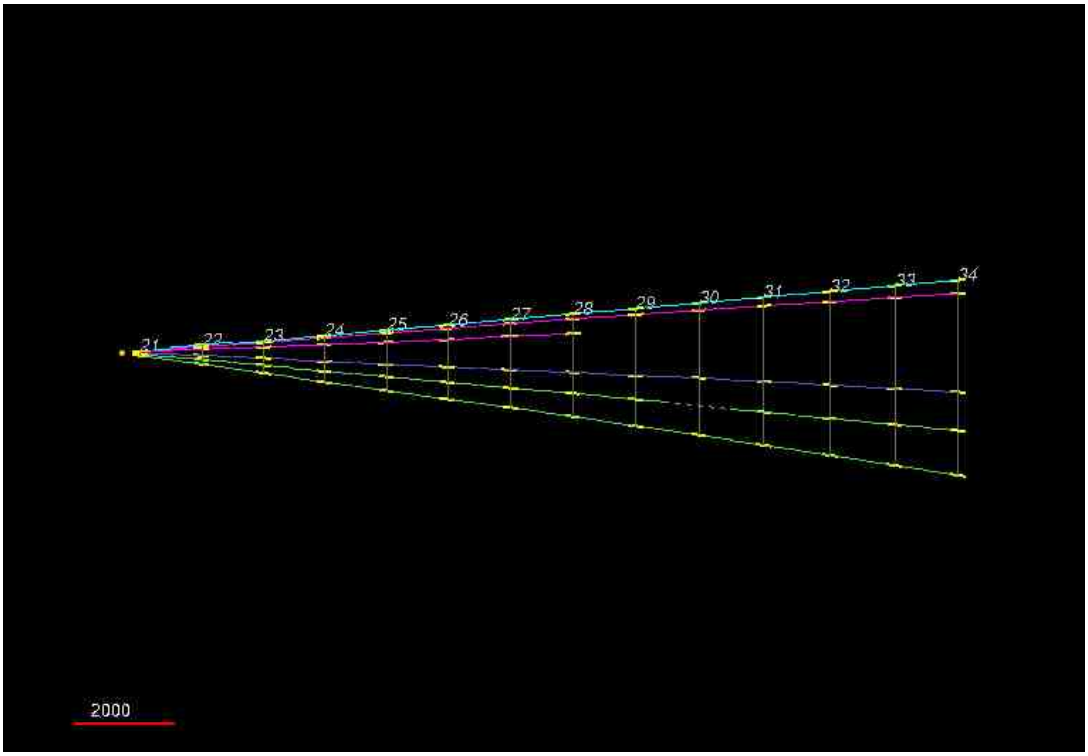

Figure A.20: A vertex with 6 tracks.